University of Alberta

Switching Rates of Dual Selection Combining in Doppler Fading Channels

by

Xin Wang

A thesis submitted to the Faculty of Graduate Studies and Research
in partial fulfillment of the requirements for the degree of

Master of Science
in
Communications

Department of Electrical and Computer Engineering

Edmonton, Alberta
Fall 2008

Library and Archives Canada

Published Heritage Branch

395 Wellington Street
Ottawa ON K1A 0N4
Canada

Bibliothèque et Archives Canada

Direction du Patrimoine de l'édition

395, rue Wellington
Ottawa ON K1A 0N4
Canada

Your file Votre référence
ISBN: 978-0-494-47439-6
Our file Notre référence
ISBN: 978-0-494-47439-6

NOTICE:
The author has granted a non-exclusive license allowing Library and Archives Canada to reproduce, publish, archive, preserve, conserve, communicate to the public by telecommunication or on the Internet, loan, distribute and sell theses worldwide, for commercial or non-commercial purposes, in microform, paper, electronic and/or any other formats.

The author retains copyright ownership and moral rights in this thesis. Neither the thesis nor substantial extracts from it may be printed or otherwise reproduced without the author's permission.

AVIS:
L'auteur a accordé une licence non exclusive permettant à la Bibliothèque et Archives Canada de reproduire, publier, archiver, sauvegarder, conserver, transmettre au public par télécommunication ou par l'Internet, prêter, distribuer et vendre des thèses partout dans le monde, à des fins commerciales ou autres, sur support microforme, papier, électronique et/ou autres formats.

L'auteur conserve la propriété du droit d'auteur et des droits moraux qui protège cette thèse. Ni la thèse ni des extraits substantiels de celle-ci ne doivent être imprimés ou autrement reproduits sans son autorisation.

In compliance with the Canadian Privacy Act some supporting forms may have been removed from this thesis.

While these forms may be included in the document page count, their removal does not represent any loss of content from the thesis.

Conformément à la loi canadienne sur la protection de la vie privée, quelques formulaires secondaires ont été enlevés de cette thèse.

Bien que ces formulaires aient inclus dans la pagination, il n'y aura aucun contenu manquant.

Canada

Abstract

Diversity plays an important role in mitigating the effects of fading and improves the system performance during signal transmission over fading channels. Selection diversity is widely employed in receivers due to its economical and practical designs. In dual selection diversity combining, the receiver chooses one diversity branch with larger amplitude from two branches. The diversity switching rate is useful in evaluating receiver outages due to switching transients. Moreover, the diversity switching rate provides useful information in the design of phase estimation in coherent demodulation. Power is also a concern in mobile terminals since switching branches consumes power. In this thesis, analytical solutions for switching rates are derived for a dual selection combiner operating on: correlated Rayleigh and Rician fading channels in a noise-free environment; independent and identically distributed (i.i.d.) κ-μ and α-μ fading channels in the absence of noise; and independent Rayleigh and Rician fading channels with consideration of noise.

Acknowledgements

I am deeply grateful to my supervisor, Dr. Norman Beaulieu for providing a valuable opportunity to work with him, and for training me as a M.Sc. student in the *i*CORE Wireless Communication Laboratory.

I would like to thank all the graduate students and staff at the *i*CORE Wireless Communication Laboratory who provided me with all technical and administrative help.

Last but not least, I owe a great deal to my family for their everlasting love and support.

Contents

1 INTRODUCTION **1**

1.1 Multipath Fading 2

1.1.1 Homogeneous Scattering Environment 2

1.1.2 Non-Homogeneous Scattering Environment 7

1.2 Dual Selection Diversity Combining 9

1.3 Thesis Outline and Contributions 10

2 Level Crossing Rate and Switching Rate **13**

2.1 Level Crossing Rate 13

2.2 Switching Rate of Dual Selection Diversity Combining 15

2.2.1 Motivation 15

2.2.2 Derivation of Switching Rate 16

3 Switching Rates of Dual Branch Selection Diversity in Correlated Doppler Fading **19**

3.1 Dual Correlated Rayleigh Fading Channels 20

3.1.1 System Model 20

3.1.2 Derivation of Analytical Expressions for Switching Rate 20

3.2 Dual Correlated Rician Fading Channels 24

3.2.1 System Model 24
3.2.2 Derivation of Analytical Expressions for Switching Rate 25
3.3 Numerical Results 26

4 Switching Rates of Two-Branch Selection Diversity in κ-μ and α-μ Distributed Fading **36**

4.1 Dual κ-μ Fading Channels 37
4.2 Dual α-μ Fading Channels 40
4.3 Numerical Results 42

5 Switching Rates of Dual Selection Diversity in Noisy Fading Channels **47**

5.1 System Model 48
5.2 Rician Fading Channels 50
5.3 Rayleigh Fading Channels 53
5.4 Numerical Results 54

6 Summary and Conclusions **60**

Appendix A Equivalence of the κ-μ Distribution and the Generalized Rician Distribution **63**

Appendix B Derivation of Conditional Mean and Variance of $\dot{S}$ in Rayleigh Fading **65**

Appendix C Derivation of Conditional Mean and Variance of $\dot{R}$ in Rician Fading **67**

References **70**

List of Figures

1.1 The multipath propagation of a signal from the transmitter to the receiver in a typical wireless environment where a LOS component exists. 3

1.2 Rayleigh fading signal envelope (mobile speed 40 km/h, carrier frequency 1.9 GHz, $b_0 = 1$). 6

1.3 Output signal envelope from a dual selection diversity combining system operating on i.i.d. Rayleigh fading branches (mobile speed 40 km/h, carrier frequency 1.9 GHz, $b_0 = 1$). 12

2.1 Normalized average envelope LCR. 15

2.2 Illustration of the switching transient in dual selection diversity combining system. 17

2.3 Illustration of the branch switchings of selection diversity combining in dual i.i.d. Rayleigh fading. 18

3.1 The antenna configuration. 28

3.2 Comparison of normalized switching rates of dual selection combining for balanced correlated Rayleigh fading branches with different values of the antenna angle, α, and dual i.i.d. fading ($\Omega_1 = \Omega_2 = 0.5$). 30

3.3 Comparison of normalized switching rates of dual selection combining for unbalanced correlated Rayleigh fading branches with different values of the antenna angle, α, and dual i.n.d. fading ($\Omega_1 = 0.1, \Omega_2 = 0.9$). 31

3.4 Comparison of normalized switching rates of dual selection combining for balanced correlated Rician fading branches with different values of the antenna angle, α, and dual i.i.d. fading ($\sigma_1 = \sigma_2$). 32

3.5 Comparison of normalized switching rates of dual selection combining for correlated Rician fading branches with equal Rice factors for different values of the antenna angle, α, and dual independent fading. 33

3.6 Comparison of normalized switching rates of dual selection combining for correlated Rician fading branches with equal scatter powers for different values of the antenna angle, α, and dual independent fading ($K_1 = 1$, $K_2 = 5$, $\sigma_1 = \sigma_2$). 34

3.7 Comparison of normalized switching rates of dual selection combining for correlated Rician fading branches with unequal scatter powers and unequal Rice factors for different values of the antenna angle, α, and dual independent fading ($K_1 = 1$, $K_2 = 5$, $c_\sigma = 1/3$). 35

4.1 Normalized switching rates of dual selection combining in i.i.d. κ-μ fading branches with fixed values of parameter, μ. 43

4.2 Normalized switching rates of dual selection combining in i.i.d. κ-μ fading branches with fixed values of parameter, κ. 44

4.3 Comparison of theoretical (dash-dotted line) and simulated (diamond) normalized switching rates of dual selection combining in i.i.d. κ-μ fading branches for $\mu = 2$. 45

4.4 Comparison of theoretical (dash-dotted line) and simulated (diamond) normalized switching rates of dual selection combining in i.i.d. α-μ fading branches. 46

5.1 Power spectral desity of received signal envelope and bandlimited Gaussian noise for a 2-D isotropic fading channel with an omnidirectional antenna (after [21, Fig. 1]). 49

5.2 Normalized switching rates of dual selection combining in i.i.d. Rayleigh fading branches in the presence of noise. 56

5.3 Normalized switching rates of dual selection combining in i.n.d. Rayleigh fading branches in the presence of noise for $c_\sigma = 0.5$ ($\gamma_1 = 4\gamma_2$). 57

5.4 Normalized switching rates of dual selection combining in i.i.d. Rician fading branches in the presence of noise when $K = 1$ (solid line), and $K = 5$ (dashed line). 58

5.5 Normalized switching rates of dual selection combining in i.n.d. Rician fading branches in the presence of noise when $K_1 = 1$, $K_2 = 5$, $c_\sigma = 1$ (solid line) and $K_1 = K_2 = 5$, $c_\sigma = 1/3$ (dashed line). 59

Acronyms

Acronyms	Definition
2-D	Two-dimensional
AWGN	Additive White Gaussian Noise
EGC	Equal Gain Combining
i.i.d.	Independent and Identically Distributed
i.n.d.	Independent and Non-identically Distributed
JPDF	Joint probability Density Function
LCR	Level Crossing Rate
LOS	Line-of-sight
MRC	Maximal Ratio Combining
PDF	Probability Density Function
PSD	Power Spectral Density
rms	Root-mean-square Value
RV	Random Variable
SC	Selection Combining
SNR	Signal-to-noise Ratio
SSC	Switch-and-stay Combining

List of Symbols

Symbol	Definition
${}_2F_2(\cdot,\cdot;\cdot,\cdot;\cdot)$	Hypergeometric function
${}_3F_3(\cdot,\cdot,\cdot;\cdot,\cdot,\cdot;\cdot)$	Hypergeometric function
a	Power in the line-of-sight component
B_w	Receiving filter bandwidth
b_n	The n^{th} moment of inphase and quadrature components ($n = 0, 1, 2, 3...$)
$\mathbf{b}$	Covariance matrix
C_n	Amplitude of n^{th} path
c_i	Received complex signal in the presence of noise
d	Antenna spacing
$\mathbb{E}(x)$	Expectation of X
f_D	Maximum Doppler frequency
$f(x)$	Probability density function of X
$f(x,y)$	Joint probability density function of X and Y
f_c	Carrier frequency
g_I	Inphase components
g_Q	Quadrature components
$I_0(\cdot)$	Modified Bessel function of the first kind of order zero
J	Jacobian of a linear transformation

$J_n(\cdot)$	The nth order Bessel function of the first kind
K	Rice factor
k	Number of multipath clusters
$\mathbf{M}$	Conditional mean
m_{gI}	Mean of inphase component
m_{gQ}	Mean of quadrature component
$\mathbf{m}$	Mean vector
m	Conditional mean
$n(t)$	Noise signal
N_0	Noise power spectral density
$N_{R_{th}}$	Average level crossing rate
p_k	Means of inpahse components of multipath waves of cluster k
q_k	Means of quadrature components of multipath waves of cluster k
R_{th}	Signal threshold
R_{rms}	*rms* value of envelope R
R_{SW}^{sc}	Selection combining switching rate
$r_i(t)$	Fading signal envelope at i^{th} antenna
$\hat{r}$	Root mean square value of R in κ-μ distribution
$\dot{r}_i(t)$	Time derivative of fading signal envelope at i^{th} antenna
$\mathbf{S}$	Signal vector
$S(f)$	Power spectral density function
$s_i(t)$	Received signal envelope at i^{th} antenna
t	Time
$\mathrm{Var}(x)$	Variance of X
X	Gaussian random variable

Y	Gaussian random variable
$Z(t)$	New random process
$z(t)$	Received complex signal
α	Angle between antenna axis and direction of vehicle motion
	Power parameter
$(\alpha)_k$	Pochhammer symbol
γ_i	Received signal-to-noise ratio at i^{th} antenna
θ_i	Phase of received complex signal envelope at i^{th} antenna
κ	Ratio between the total power in the LOS components and the total power in the scattering components in κ-μ distribution
Λ	Conditional variance
λ_c	Wavelength of carrier frequency
μ	Real extension of the integer n
ν	Mobile speed
ρ	Normalized signal level
ρ_{12}	Crosscorrelation coefficient
σ_i^2	Power in scattering components at i^{th} antenna
$\dot{\sigma}_i^2$	Variance of time derivative of received signal at i^{th} antenna
τ	Time delay
$\phi_n(t)$	Random phase
$\Phi(\tau)$	Autocorrelation function
Ω_z	Average received signal power
Ω_i	Average received signal power at i^{th} antenna

Chapter 1

INTRODUCTION

The 21^{st} century witnesses the dramatically increasing demands of wireless technology, which makes the workforce and the individual more mobile. Human beings benefit a lot from wireless products, such as cellular phones, personal digital assistant (PDA), Global Positioning System (GPS), etc. Current wireless systems give people easy access to multimedia, such as voice, video and television when they are walking on the streets, driving on the highways and even traveling around the world. The fundamental requirement of the wireless technology is to provide high data rate. Meanwhile, limited spectral resources and exponentially growing population create many unsolved problems which make future wireless communications both challenging and intriguing. For instance, designing receiver systems to combat fading, which affects the quality of mobile service, arouses my research interest.

This chapter is organized as follows. Section 1.1 introduces the multipath fading environment and the system models adopted in this thesis. In Section 1.2, dual selection diversity combining scheme is presented. Section 1.3 outlines my thesis and summarizes the contributions.

1.1 Multipath Fading

In wireless transmission environments, the signal may take many paths from the transmitter to the receiver, including reflections and refractions caused by the local terrain features. Fig. 1.1 shows the multipath propagation of a signal from the transmitter to the mobile terminal in a wireless environment and a line-of-sight (LOS) path is present. In typical urban propagation environments, the transmitted signal undergoes much scattering before arriving at the receiver. At the receiver, the multiple replicas of the transmitted signal can add constructively and destructively. Thus, the received signal is a complex combination of variations of the received signal envelope, frequency and phase. The resultant signal fades rapidly and is characterized as short-term fading, which is considered in this thesis.

The relative motion between the mobile terminal and the base station causes frequency shift of the received signal. This frequency shift is due to the Doppler effect, which is directly proportional to mobile speed. As the result of the Doppler shift, the bandwidth of the received signal is expanded. This phenomenon as well as the bandwidth of fading channel leads to the different types of fading. When the signal bandwidth is less than the channel coherence bandwidth, all frequencies in the transmitted signal have the same gain and phase shift due to multipath fading. This kind of channel introduces very little distortion of the desired signal, and this is known as flat fading. When the signal bandwidth is larger than the channel coherence bandwidth, the frequency components experience significantly different phase shifts and the signal amplitude varies as a function of frequency. This is known as frequency selective fading. In this thesis, we only consider flat fading.

1.1.1 Homogeneous Scattering Environment

Statistical models are commonly used to characterize the fading channels. We assume that the transmitted signals are vertically polarized and the signal propagation environment is

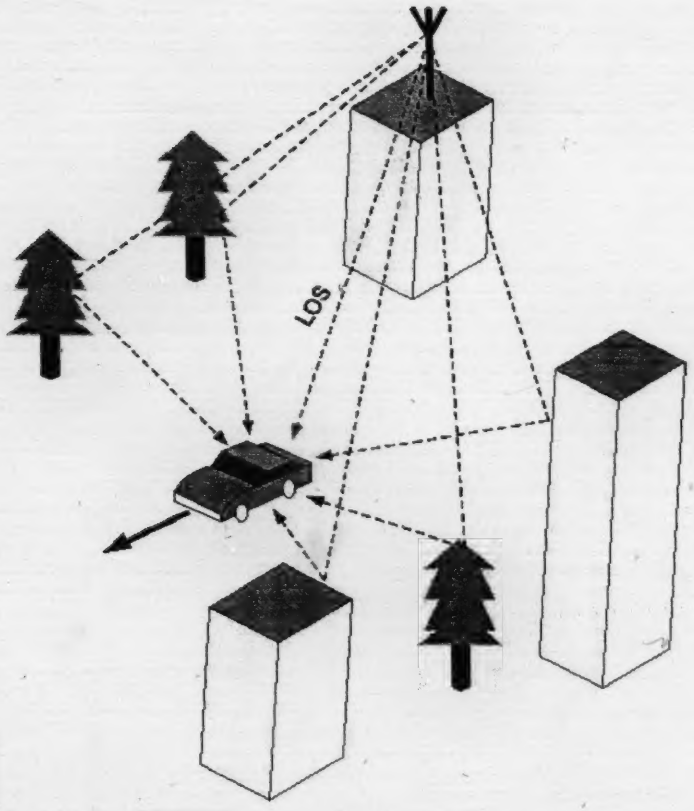

Fig. 1.1. The multipath propagation of a signal from the transmitter to the receiver in a typical wireless environment where a LOS component exists.

modeled as two-dimensional (2-D) [1]. The received band-pass signal can be expressed in the quadrature form as [1, eq. (2.10)]

$$z(t) = g_I(t)\cos 2\pi f_c t - g_Q(t)\sin 2\pi f_c t \tag{1.1}$$

where

$$g_I(t) = \sum_{n=1}^{N} C_n \cos\phi_n(t) \tag{1.2a}$$

$$g_Q(t) = \sum_{n=1}^{N} C_n \sin\phi_n(t) \tag{1.2b}$$

are the inphase and quadrature components, f_c is the carreir frequency, C_n is the amplitude of the n^{th} path, and $\phi_n(t)$ is the random phase. For sufficient large N, the central-limit theorem leads $g_I(t)$ and $g_Q(t)$ to approximate Gaussian random processes.

Let $\mathbb{E}(\cdot)$ denote the expectation, and the autocorrelation function of the received signal $z(t)$ is defined as

$$\begin{aligned}\Phi_{zz}(\tau) &= \mathbb{E}[z(t)z(t+\tau)]/2 \\ &= \Phi_{g_Ig_I}(\tau)\cos 2\pi f_c\tau - \Phi_{g_Qg_I}(\tau)\sin 2\pi f_c\tau. \end{aligned} \tag{1.3}$$

where

$$\Phi_{g_Ig_I}(\tau) = \Phi_{g_Qg_Q}(\tau) \tag{1.4a}$$

$$\Phi_{g_Qg_I}(\tau) = \Phi_{g_Ig_Q}(-\tau) \tag{1.4b}$$

and τ is the time delay. With 2-D isotropic scattering and an omnidirectional receiver antenna, (1.4a) can be evaluated as

$$\Phi_{g_Ig_I}(\tau) = \frac{\Omega_z}{2} J_0(2\pi f_D\tau) \tag{1.5}$$

where Ω_z is the average received signal power, $J_0(\cdot)$ is the zero-order Bessel function of the first kind and f_D is the maximum Doppler frequency defined as

$$f_D = \frac{v}{\lambda_c} \tag{1.6}$$

where v is mobile speed and λ_c is the wavelength of the carrier. The crosscorrelation, (1.4b), becomes zero, which means that the inphase and quadrature components are uncorrelated Gaussian random processes.

The power spectral density (PSD) function of $z(t)$ is the Fourier transform of its autocorrelation function given by

$$S_{zz}(f) = \frac{\Omega_z}{4\pi f_D} \frac{1}{\sqrt{1-\left(\frac{f-f_c}{f_D}\right)^2}}, \quad |f-f_c| \le f_D. \tag{1.7}$$

The n^{th} spectral moment of the inphase and quadrature components, b_n, $n = 0,\ 1,\ 2,\ \cdots$, can be obtained from the PSD as

$$b_n = (2\pi)^n \int_{f_c - f_D}^{f_c + f_D} f^n S_{zz}(f)(f - f_c)^n \mathrm{d}f. \tag{1.8}$$

Substituting (1.7) into (1.8) yields

$$b_n = \begin{cases} b_0 (2\pi f_D)^n \frac{1 \cdot 3 \cdot 5 \cdots (n-1)}{2 \cdot 4 \cdot 6 \cdots n} & n \text{ even} \\ 0 & n \text{ odd}, \end{cases} \tag{1.9}$$

where $b_0 = \Phi_{g_I g_I}(0)$.

1.1.1.1 Rayleigh Fading

The received signal envelope can be written in complex form as

$$z(t) = g_I(t) + j g_Q(t) = r(t) \mathrm{e}^{j\theta(t)}, \tag{1.10}$$

where $r(t)$ and $\theta(t)$ are the envelope and the phase of $z(t)$, respectively, and $j^2 = -1$. Under 2-D isotropic scattering conditions, $g_I(t)$ and $g_Q(t)$ are mutually independent identically distributed Gaussian random variables (RVs) at any time instant t with

$$\mathbb{E}[g_I] = \mathbb{E}[g_Q] = 0 \tag{1.11}$$

$$\mathrm{Var}[g_I] = \mathrm{Var}[g_Q] = b_0 \tag{1.12}$$

where Var[·] denotes variance. Then, r has the Rayleigh distribution with probability density function (PDF) given by

$$f_R(r) = \frac{r}{b_0} \exp\left(-\frac{r^2}{2b_0}\right), \quad r \geq 0. \tag{1.13}$$

The average power in r is $\mathbb{E}[R^2] = 2b_0$. Fig. 1.2 shows a typical Rayleigh fading envelope generated by the fading channel simulator [2], whose statistical quality was documented according to the methods described in [3].

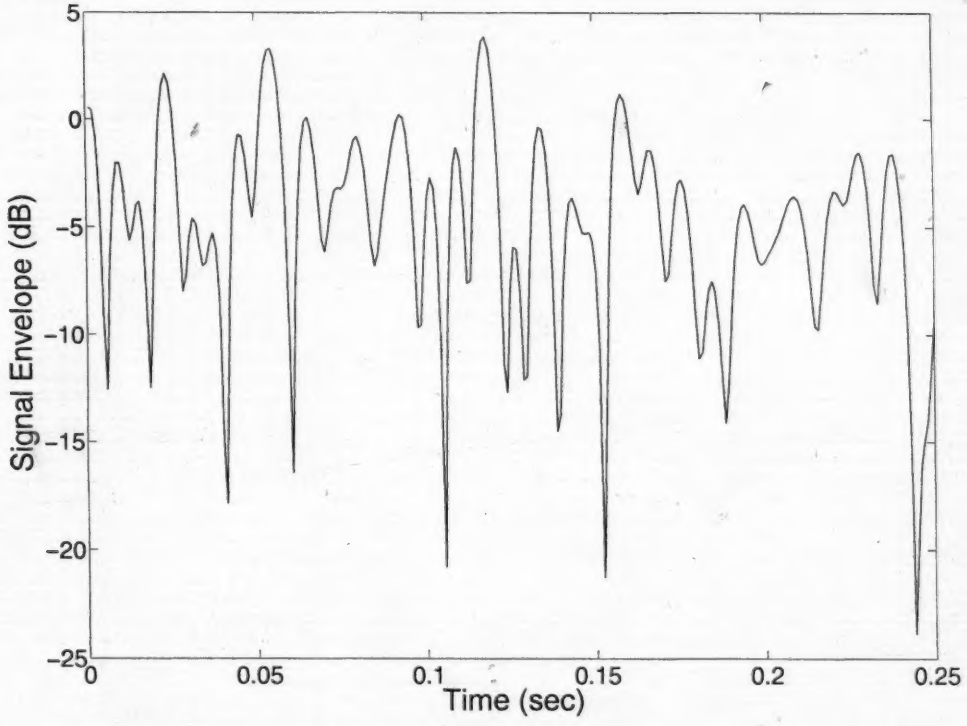

Fig. 1.2. Rayleigh fading signal envelope (mobile speed 40 km/h, carrier frequency 1.9 GHz, $b_0 = 1$).

1.1.1.2 Rician Fading

In the case where $g_I(t)$ and $g_Q(t)$ are mutually independent identically distributed Gaussian RVs with non-zero means, m_{g_I} and m_{g_Q}, respectively, i.e. there exists a specular or a LOS component, the fading is no longer described by the Rayleigh distribution. We again assume that $g_I(t)$ and $g_Q(t)$ have identical variance b_0. Then the magnitude of the received complex envelope has a Rician distribution with PDF given by

$$f_R(r) = \frac{r}{b_0}\exp\left(-\frac{r^2+a^2}{2b_0}\right) I_0\left(\frac{ar}{b_0}\right), \quad r \geq 0 \tag{1.14}$$

where

$$a^2 = m_{gI}^2 + m_{gQ}^2 \tag{1.15}$$

is the power in the LOS component, and $I_0(\cdot)$ is the zero-order modified Bessel function of the first kind [4]. The Rice factor, K, is defined as the ratio of the power in the LOS component to the power in the scattering component given by

$$K = \frac{a^2}{2b_0}. \tag{1.16}$$

Then (1.14) can be written as

$$f_R(r) = \frac{r}{b_0}\exp\left(-\frac{r^2}{2b_0} - K\right) I_0\left(\frac{r}{b_0}\sqrt{2K}\right), \quad r \geq 0. \tag{1.17}$$

Setting $K = 0$ yields Rayleigh fading since $I_0(0) = 1$.

1.1.2 Non-Homogeneous Scattering Environment

1.1.2.1 κ-μ Fading

Recently, [5] has proposed the κ-μ distribution as a fading model which describes the short term signal variation of a fading signal in the presence of LOS components. The κ-μ distribution is more realistic than other traditional distributions, such as Rayleigh, Rician and Nakagami-m distributions, since its derivation is completely based on a non-homogeneous scattering environment. The κ-μ distribution is a general physical fading model which includes Rayleigh, Rician, and Nakagami-m fading models as special cases. This fading model considers clusters of multipath waves propagating over a non-homogeneous environment and the received envelope, R, can be modeled in terms of the in-phase and quadrature components as

$$R = \sqrt{\sum_{k=1}^{n}(X_k + p_k)^2 + \sum_{k=1}^{n}(Y_k + q_k)^2} \tag{1.18}$$

where X_k and Y_k are mutually independent zero-mean Gaussian random processes with $\mathbb{E}[X_k^2] = \mathbb{E}[Y_k^2] = \sigma^2$, p_k and q_k are the means of the inphase and quadrature components of the multipath waves of cluster k, respectively, and k is the number of multipath clusters. Then κ is defined as the ratio between the total power in the LOS components and the total power in the scattering components [6]

$$\kappa = \frac{a^2}{2n\sigma^2} \tag{1.19}$$

where

$$a^2 = \sum_{k=1}^{n} (p_k^2 + q_k^2).$$

The κ-μ distribution is also known as the generalized Rician distribution (see Appendix A).

The PDF of the κ-μ distribution is given by [5]

$$\begin{aligned} f_R(r) = & \frac{2\mu(1+\kappa)^{\frac{\mu+1}{2}}}{\hat{r}\kappa^{\frac{\mu-1}{2}}\exp(\mu\kappa)} \left(\frac{r}{\hat{r}}\right)^{\mu} \\ & \times \exp\left[-\mu(1+\kappa)\left(\frac{r}{\hat{r}}\right)^2\right] I_{\mu-1}\left[2\mu\sqrt{\kappa(1+\kappa)}\frac{r}{\hat{r}}\right] \end{aligned} \tag{1.20}$$

where

$$\hat{r} = \sqrt{\mathbb{E}[R^2]} = \sqrt{2n\sigma^2 + a^2}$$

is the *rms* (root mean square) value of R, $\kappa > 0$, and $\mu > 0$ is the real extension of integer n.

1.1.2.2 α-μ Fading

Another useful fading model that has been reported recently is the α-μ model. The derivation of α-μ fading model is based on considering clusters of multipath waves propagating in a non-homogeneous environment, and it is actually a version of the generalized Gamma distribution [7].

The received α-μ fading signal envelope including n multipath clusters is given in [8]

$$R^{\alpha} = \sum_{k=1}^{n} (X_k^2 + Y_k^2) \tag{1.21}$$

where $\alpha > 0$ is the power parameter, and X_k and Y_k are mutually independent zero-mean Gaussian random processes with $\mathrm{Var}[X_k] = \mathrm{Var}[Y_k] = \sigma^2$. The corresponding PDF of the α-μ distribution is given in [8]

$$f_R(r) = \frac{\alpha \mu^{\mu} r^{\alpha\mu-1}}{\hat{r}^{\alpha\mu}\Gamma(\mu)} \exp\left(-\frac{\mu r^{\alpha}}{\hat{r}^{\alpha}}\right) \tag{1.22}$$

where $\mu > 0$ is a real extension of the integer n, given by inverse of the normalized variance of R^{α}

$$\mu = \frac{\mathbb{E}^2[R^{\alpha}]}{\mathrm{Var}[R^{\alpha}]},$$

and

$$\hat{r} = \sqrt[\alpha]{\mathrm{E}[R^{\alpha}]} = \sqrt[\alpha]{2\mu\sigma^2}$$

is the α-root mean value of R^{α}.

1.2 Dual Selection Diversity Combining

There are several combining techniques used to improve the signal quality, such as selection combining (SC), switch-and-stay combining (SSC), maximal ratio combining (MRC) and equal gain combining (EGC). Selection combining diversity is the simplest technique of all and widely employed in receiver designs to mitigate the effects of deep fading. The principle of selection combining diversity is that the probability of multiple received signals being in deep fades simultaneously is much smaller than that of a single branch being in a deep fade, and the power of the resulting signal is strengthened. In dual selection combining diversity, the receiver chooses one diversity branch with larger signal amplitude from two

received fading branches. The output signal envelope from the selection diversity combiner at time t can be expressed as

$$r(t) = \max\{r_1(t), r_2(t)\} \tag{1.23}$$

where $r_1(t)$ is the received signal at antenna 1 and $r_2(t)$ is the received signal at antenna 2 at time t. Fig. 1.3 shows the resulting signal from the selection diversity combiner. It is observed that the output signal designated by the solid line has shallower fades than either branch 1 designated by the dash-dotted line or branch 2 shown by a dashed line has, and the power in the output signal is much stronger than that in either branch.

1.3 Thesis Outline and Contributions

The remainder of this thesis is organized as follows. In Chapter 2, we introduce the most important concept, level crossing rate (LCR), behind the switching rate of selection diversity combining. The idea of the switching rate arises from the concept of LCR.

In Chapter 3, an analytical solution for the switching rate of a correlated dual branch selection diversity combiner in Rayleigh and Rician fading is derived in the absence of noise. Balanced and unbalanced branches are considered. Numerical results are also presented for a space-diversity system with horizontally spaced omnidirectional antennas at a mobile station.

In Chapter 4, a closed-form expression for the switching rate of a dual branch selection diversity combiner operating on κ-μ and α-μ distributed fading channels is derived. Independent and identical distributed (i.i.d.) κ-μ as well as α-μ fading channels without noise are adopted. The switching rates for dual i.i.d. Rayleigh, Rician and Nakagami-m fading channels are special cases of the switching rate for dual i.i.d. κ-μ fading channels. Similarly, the general switching rates for dual α-μ fading channels also include special

cases such as Rayleigh and Nakagami-m fading channels.

To this point in the thesis, we have only considered noise-free conditions in the derivation of the switching rates. In real wireless communication systems, however, noise is unavoidable and it degrades the quality of the received signal. In Chapter 5, the impact of noise on the switching rate of a dual branch selection diversity combiner is examined. A closed-form solution is derived for i.i.d. and independent and non-identically distributed (i.n.d.) fading channels. The switching rate in noisy fading channels is compared to that in noise-free conditions. At high signal-to-noise ratio (SNR), the switching rate in noisy fading channels converges to that in a noise-free environment, as expected.

In the last chapter, we present a summary of this thesis and draw some conclusions.

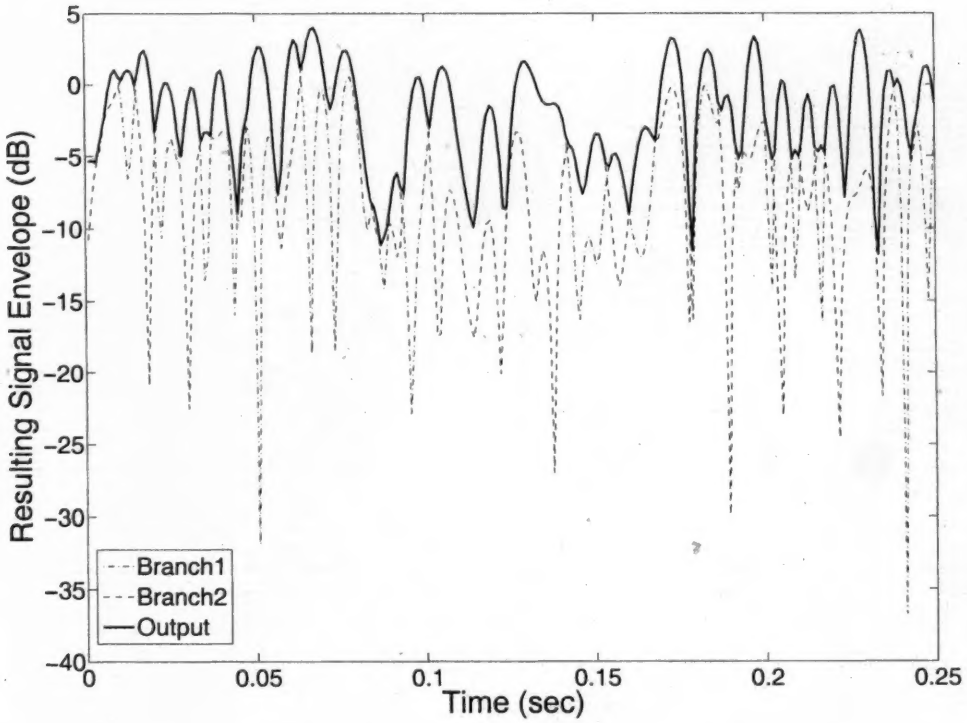

Fig. 1.3. Output signal envelope from a dual selection diversity combining system operating on i.i.d. Rayleigh fading branches (mobile speed 40 km/h, carrier frequency 1.9 GHz, $b_0 = 1$).

Chapter 2

Level Crossing Rate and Switching Rate

The principle behind the concept of the switching rate is the level crossing rate (LCR). From Fig. 1.2, one can see the rapid fluctuations of a fading signal. The rate at which the time-varying amplitude of the faded signal crosses a threshold, or the level crossing rate, provides useful information for wireless system design engineers. This rate is random and, thus, its full characteristic would be given by the PDF of the level crossing rate. Yet, all that is known theoretically is the average level crossing rate, which is the first moment of the level crossing rate distribution. Therefore, the switching rate of selection diversity combining derived in this thesis is also the first moment of the switching rate distribution.

2.1 Level Crossing Rate

The level crossing rate at a threshold, R_{th}, is defined as the rate at which the fading signal amplitude crosses level, R_{th}, in a positive-going or negative-going direction. There is a large body of literature on the level crossing rate because of its practical importance. Let $\dot{r}$ denote derivative with respect to time, t, of r and the average level crossing rate, $N_{R_{th}}$, is given by [9]

$$N_{R_{th}} = \int_0^\infty \dot{r} f(r = R_{th}, \dot{r}) \mathrm{d}\dot{r} \tag{2.1}$$

where $f(r,\dot{r})$ is the joint probability density function (JPDF) of r and $\dot{r}$. (2.1) is a general expression that can be applied to any random process.

The JPDF $f(r,\dot{r})$ for a sine wave plus narrow-band Gaussian noise has been derived by Rice [1, eq. (2.91)]

$$\begin{aligned} f(r,\dot{r}) = & \frac{r(2\pi)^{-3/2}}{\sqrt{Bb_0}} \int_{-\pi}^{\pi} \mathrm{d}\theta \\ & \times \exp\left\{ -\frac{1}{2Bb_0} \left[B(r^2 - 2ra\cos\theta + a^2) + (b_0\dot{r} + b_1 a \sin\theta)^2 \right] \right\} \end{aligned} \tag{2.2}$$

where a is defined in (1.15) and $B = b_0 b_2 - b_1^2$ and b_n is given in (1.8). For 2-D isotropic scattering, (2.2) can be evaluated as [1, eq. (2.97)]

$$\begin{aligned} f(r,\dot{r}) &= \sqrt{\frac{1}{2\pi b_2}} \exp\left(-\frac{\dot{r}^2}{2b_2} \right) \cdot \frac{r}{b_0} \exp\left(-\frac{r^2 + a^2}{2b_0} \right) I_0\left(\frac{ra}{b_0} \right) \\ &= f(\dot{r}) \cdot f(r). \end{aligned} \tag{2.3}$$

Apparently, it follows that r and $\dot{r}$ are independent from the above result. Substituting (2.3) into (2.1) gives the average LCR of Rician fading [1, eq. (2.99)]

$$N_R = \sqrt{2\pi(K+1)} f_D \, \rho \, \exp\left[-K - (K+1)\rho^2 \right] I_0\left(2\rho\sqrt{K(K+1)} \right) \tag{2.4}$$

where

$$\rho = \frac{R_{th}}{R_{rms}} \tag{2.5}$$

and $R_{rms} = \sqrt{\Omega_z}$ is the *rms* value of envelope. For Rayleigh fading, $K = 0$, (2.4) simplifies to

$$N_{R_{th}} = \sqrt{2\pi} f_D \, \rho \, \exp\left(-\rho^2 \right). \tag{2.6}$$

Fig. 2.1 shows plots of the normalized average envelope LCR as a function of ρ and K. When $K = 0$, it specialized to the normalized average envelope LCR for Rayleigh fading.

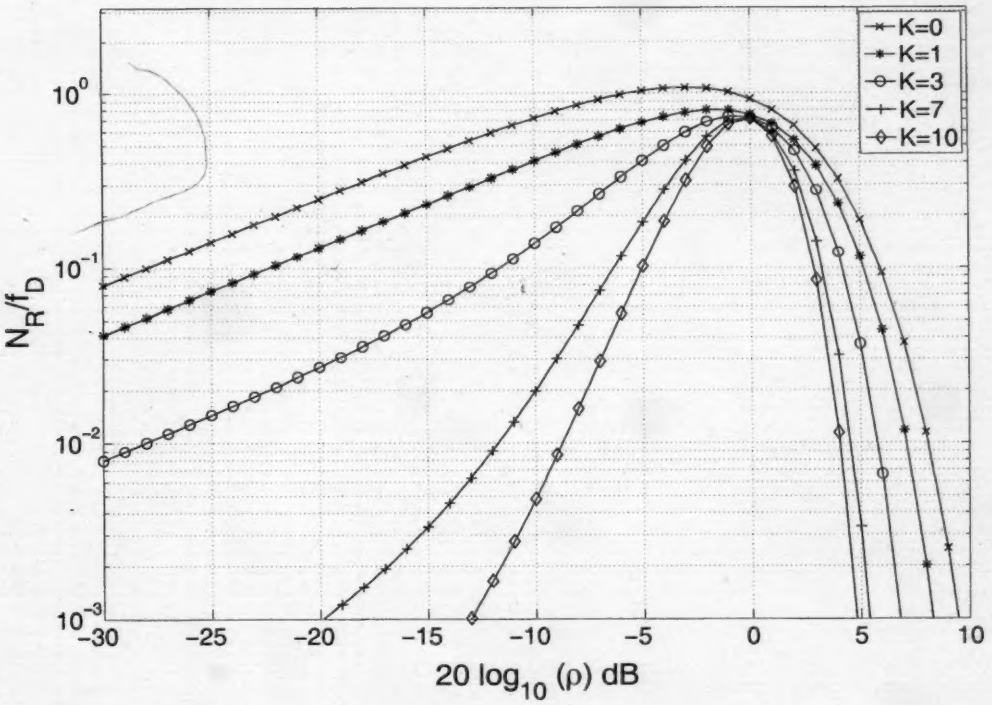

Fig. 2.1. Normalized average envelope LCR.

2.2 Switching Rate of Dual Selection Diversity Combining

2.2.1 Motivation

In dual selection combining diversity system, the combiner selects one diversity branch with larger signal envelope from two available branches. The switching rate of the diversity combining is required for evaluating receiver outages due to switching transients. That is, execution of switching antennas causes a transient in the receiver circuits, and the transient will corrupt any data signal present at the same time. If the receiver switches too often, much of the desired data can be lost due to the fact that each switching transient corrupts

the receiver filters [10], which is illustrated in Fig. 2.2. Also importantly, the switching rate provides useful information in the design of phase estimation in coherent demodulation receivers for system engineers. A coherent receiver needs to dwell on the received signal for some time in order to establish an accurate phase estimate for fading compensation. If the receiver encounters a very fast switching rate, there will not be adequate time for the receiver to produce an accurate phase estimate. Whether branch selection is implemented on a symbol, multiple symbol, block or frame basis is determined by the switching rate for accurate phase estimates [10], [11]. Power consumption is also a concern in battery-powered mobile terminals since the operation of switching branches consumes power [12].

2.2.2 Derivation of Switching Rate

We consider two diversity branches with fading processes $R_1(t)$ and $R_2(t)$. Form a new random process

$$Z(t) = R_1(t) - R_2(t). \tag{2.7}$$

Note that a zero-crossing from $Z(t) < 0$ to $Z(t) > 0$ corresponds to a state where $R_1(t)$ is greater than $R_2(t)$ following a state where $R_2(t)$ is greater than $R_1(t)$. This enables the receiver to switch from antenna two to antenna one. In the same manner, a zero-crossing from $Z(t) > 0$ to $Z(t) < 0$ leads to the receiver switching from antenna one to antenna two. Therefore, positive zero-crossings of $Z(t)$ correspond to the receiver switching from antenna two to antenna one, and negative zero-crossings of $Z(t)$ correspond to the receiver switching from antenna one to antenna two. Fig. 2.3 illustrates the branch switchings of dual selection diversity combining in dual i.i.d. Rayleigh fading. It is straightforward to observe when the switching occurs.

Let $\dot{Z}(t)$, $\dot{R}_1(t)$ and $\dot{R}_2(t)$ denote derivatives with respect to time, t, of $Z(t)$, $R_1(t)$ and $R_2(t)$, respectively. The selection combining switching rate, R_{SW}^{sc}, equals the sum of the

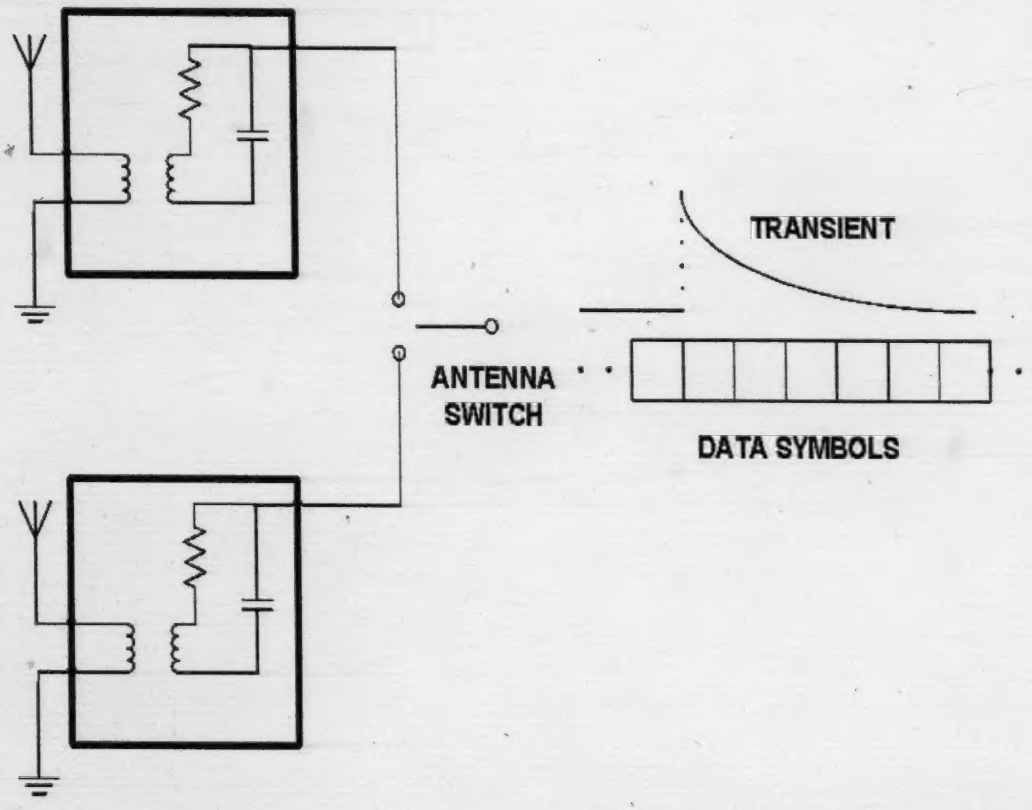

Fig. 2.2. Illustration of the switching transient in dual selection diversity combining system.

zero-crossing rates in both the negative-going and positive-going directions given by [10]

$$R_{SW}^{sc} = \int_{-\infty}^{0} |\dot{z}| f_{Z\dot{Z}}(z=0,\dot{z})\mathrm{d}\dot{z} + \int_{0}^{\infty} \dot{z} f_{Z\dot{Z}}(z=0,\dot{z})\mathrm{d}\dot{z} \tag{2.8}$$

where $f(z,\dot{z})$ is the JPDF of z and $\dot{z}$. For time-continuous signals, the negative-going and positive-going crossing rates are identical due to physical symmetry. Thus, (2.8) can be further simplified as

$$R_{SW}^{sc} = 2\int_{0}^{\infty} \dot{z} f_{Z\dot{Z}}(z=0,\dot{z})\mathrm{d}\dot{z}. \tag{2.9}$$

Eq. (2.9) is a general expression for switching rate of dual selection diversity combining

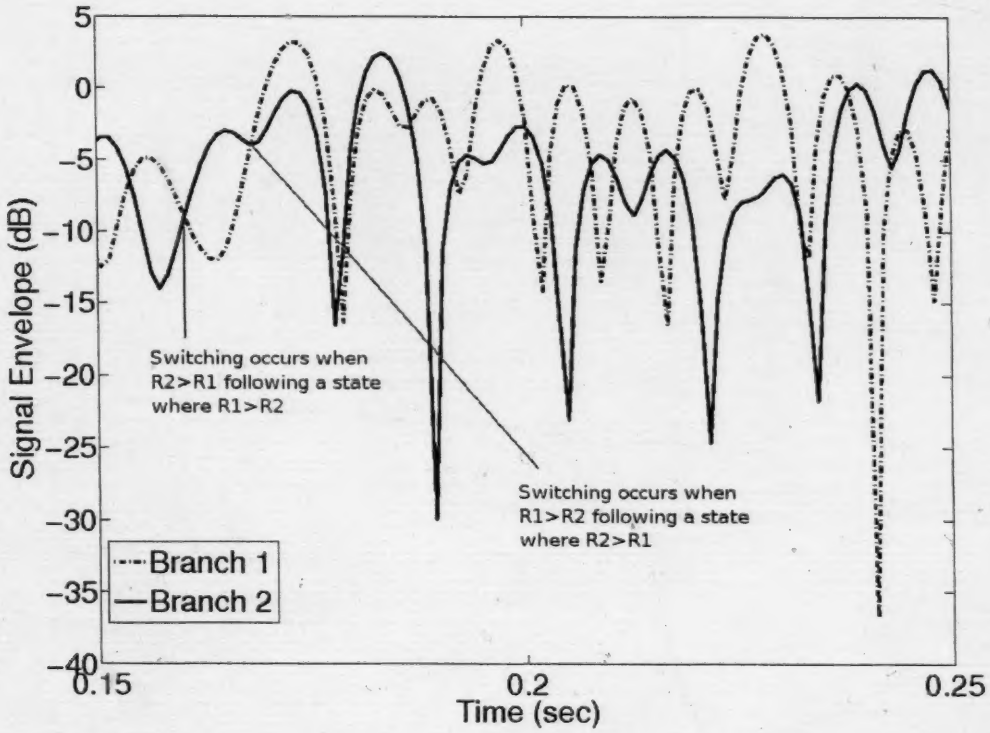
Signal Envelope (dB)
Time (sec)
Switching occurs when R2>R1 following a state where R1>R2
Switching occurs when R1>R2 following a state where R2>R1
Branch 1
Branch 2

Fig. 2.3. Illustration of the branch switchings of selection diversity combining in dual i.i.d. Rayleigh fading.

applied to any fading scenario.

Chapter 3

Switching Rates of Dual Branch Selection Diversity in Correlated Doppler Fading

Published literature on selection diversity switching rate is rare. References [11] and [13] examined the switching rate of a selection diversity receiver where M out of N independent diversity branches are combined, and references [10] and [14] studied the switching rate of dual selection diversity combining. Both of them, however, considered only independent diversity branches. Reference [12] examined a parameter called the "switching rate", which is different from the switching rate studied in this paper. The so-called "switching rate" in [12] applies to a particular discrete time implementation of selection combining or switched diversity, while the switching rate in this thesis considers the continuous time scenario, as also examined in [10], [11], [13] and [14]. References [15], [16] and [17] examined the average LCR of the output signal from a dual diversity combiner in correlated Rayleigh and Rician fading channels, but did not examine the switching rate.

In practical communication systems, the fading signals received at the different anten-

nas may be correlated. If space diversity is used at a mobile station, the average LCR will be affected by the angle between the direction of vehicle motion and the axis of the antenna array [15]. In this chapter, we consider restricted space applications, where the correlation between the two fading branches must be taken into account. A closed-form expression for the selection diversity switching rate is derived for dual correlated fading channels in the absence of noise. Both balanced and unbalanced Rayleigh and Rician fading channels are considered. Numerical results are presented for a space-diversity system with horizontally spaced omnidirectional antennas at a mobile terminal.

3.1 Dual Correlated Rayleigh Fading Channels

3.1.1 System Model

The state-of-the-art theory on switching rates presently considers only the noiseless channels [10], [11]. Chapter 5 will investigate the case with noise. In a noise-free Rayleigh fading channel, the normalized received complex signal envelope at the i^{th} antenna ($i = 1, 2$) is modeled as [16]

$$S_i(t) = \frac{R_i(t)}{\sqrt{\Omega_i}} e^{j\Theta_i(t)}, \quad R_i > 0 \tag{3.1}$$

where t denotes time, $S_i(t)$ is a zero-mean complex Gaussian random process with unit variance, $R_i(t)$ has a Rayleigh distribution with average power $\Omega_i = \mathbb{E}[R_i^2]$ and the phase $\Theta_i(t)$ is uniformly distributed on $(0,\ 2\pi]$.

3.1.2 Derivation of Analytical Expressions for Switching Rate

Define $\Theta_{12} = \Theta_2 - \Theta_1$. Then

$$f_{Z\dot{Z}}(0,\dot{z}) = \int_0^{2\pi} \int_0^{\infty} f_{\dot{Z}ZR_1\Theta_{12}}(\dot{z}, r_1 - r_2 = 0, r_1, \theta_{12}) \mathrm{d}r_1 \mathrm{d}\theta_{12} \tag{3.2}$$

where $f_{\dot{Z}ZR_1\Theta_{12}}(\dot{z}, z, r_1, \theta_{12})$ is the JPDF of $\dot{Z}$, Z, R_1 and Θ_{12}. Define the four-dimensional transformation

$$\dot{Z} = \dot{Z} \tag{3.3a}$$

$$R_1 = R_1 \tag{3.3b}$$

$$R_2 = R_1 - Z \tag{3.3c}$$

$$\Theta_{12} = \Theta_{12}. \tag{3.3d}$$

The Jacobian of the transformation (3.3) is given by [18]

$$\mathbf{J}(\dot{Z}, R_1, R_2, \Theta_{12}) = \begin{vmatrix} \frac{\partial \dot{Z}}{\partial \dot{Z}} & \frac{\partial \dot{Z}}{\partial R_1} & \frac{\partial \dot{Z}}{\partial R_2} & \frac{\partial \dot{Z}}{\partial \Theta_{12}} \\ \frac{\partial R_1}{\partial \dot{Z}} & \frac{\partial R_1}{\partial R_1} & \frac{\partial R_1}{\partial R_2} & \frac{\partial R_1}{\partial \Theta_{12}} \\ \frac{\partial Z}{\partial \dot{Z}} & \frac{\partial Z}{\partial R_1} & \frac{\partial Z}{\partial R_2} & \frac{\partial Z}{\partial \Theta_{12}} \\ \frac{\partial \Theta_{12}}{\partial \dot{Z}} & \frac{\partial \Theta_{12}}{\partial R_1} & \frac{\partial \Theta_{12}}{\partial R_2} & \frac{\partial \Theta_{12}}{\partial \Theta_{12}} \end{vmatrix} \tag{3.4}$$

where $\left| \cdot \right|$ denotes determinant. Combining (3.3) and (3.4) yields

$$\mathbf{J}(\dot{Z}, R_1, R_2, \Theta_{12}) = \begin{vmatrix} 1 & 0 & 0 & 0 \\ 0 & 1 & 0 & 0 \\ 0 & 1 & -1 & 0 \\ 0 & 0 & 0 & 1 \end{vmatrix} = -1. \tag{3.5}$$

Now, we obtain

$$\begin{aligned} f_{\dot{Z}R_1R_2\Theta_{12}}(\dot{z}, r_1, r_2, \theta_{12}) &= \left|\mathbf{J}(\dot{Z}, R_1, R_2, \Theta_{12})\right| f_{\dot{Z}R_1Z\Theta_{12}}(\dot{z}, r_1, r_1 - r_2, \theta_{12}) \\ &= f_{\dot{Z}R_1Z\Theta_{12}}(\dot{z}, r_1, r_1 - r_2, \theta_{12}). \end{aligned} \tag{3.6}$$

Since $Z = R_1 - R_2 = 0$ is required, (3.6) can be written as

$$f_{\dot{Z}R_1R_2\Theta_{12}}(\dot{z}, r_1, r_2 = r_1, \theta_{12}) = f_{\dot{Z}R_1Z\Theta_{12}}(\dot{z}, r_1, 0, \theta_{12}). \tag{3.7}$$

Substituting (3.7) into (3.2) gives

$$f_{Z\dot{Z}}(0,\dot{z}) = \int_0^{2\pi}\int_0^{\infty} f_{\dot{Z}R_1R_2\Theta_{12}}(\dot{z}, r_1, r_2 = r_1, \theta_{12})\mathrm{d}r_1\mathrm{d}\theta_{12} \tag{3.8}$$

where $f_{\dot{Z}R_1R_2\Theta_{12}}(\dot{z}, r_1, r_2, \theta_{12})$ is the JPDF of $\dot{Z}$, R_1, R_2 and Θ_{12}.

Combining the identity $f_{\dot{Z}R_1R_2\Theta_{12}}(\dot{z}, r_1, r_2, \theta_{12}) = f_{\dot{Z}|R_1R_2\Theta_{12}}(\dot{z}|r_1, r_2, \theta_{12}) f_{R_1R_2\Theta_{12}}(r_1, r_2, \theta_{12})$ with (2.9) and (3.8) yields

$$\begin{aligned} R_{SW}^{sc} = 2\int_0^{2\pi}\int_0^{\infty}\int_0^{\infty} \dot{z} f_{\dot{Z}|R_1R_2\Theta_{12}}(\dot{z}|r_1, r_2 = r_1, \theta_{12})\mathrm{d}\dot{z} \\ \times f_{R_1R_2\Theta_{12}}(r_1, r_2 = r_1, \theta_{12})\mathrm{d}r_1\mathrm{d}\theta_{12}. \end{aligned} \tag{3.9}$$

Next, we will find the expressions for $f(\dot{z}|r_1, r_2 = r_1, \theta_{12})$ and $f(r_1, r_2 = r_1, \theta_{12})$, respectively.

The JPDF of R_1, R_2, Θ_{12} is given by [16]

$$\begin{aligned} f_{R_1R_2\Theta_{12}}(r_1, r_2, \theta_{12}) = \frac{2r_1r_2}{\Omega_1\Omega_2\pi(1-|\rho_{12}|^2)} \\ \times \exp\left[-\frac{\frac{r_1^2}{\Omega_1} + \frac{r_2^2}{\Omega_2} - \frac{2r_1r_2}{\sqrt{\Omega_1\Omega_2}}\mathrm{Re}\left[\rho_{12}^* e^{j\theta_{12}}\right]}{1-|\rho_{12}|^2}\right] \end{aligned} \tag{3.10}$$

where

$$\rho_{12}(\tau) = \mathbb{E}[S_1^*(t)S_2(t+\tau)]$$

is the crosscorrelation coefficient between S_1 and S_2, and

$$\rho_{12} = \rho_{12}(0).$$

Now $f_{\dot{Z}|R_1R_2\Theta_{12}}(\dot{z}|r_1, r_2, \theta_{12})$ is given by [15]

$$\begin{aligned} f_{\dot{Z}|R_1R_2\Theta_{12}}(\dot{z}|r_1, r_2, \theta_{12}) = \frac{1}{\sqrt{2\pi\dot{\sigma}^2(r_1, r_2, \theta_{12})}} \\ \times \exp\left\{-\frac{[\dot{z} - \dot{m}(r_1, r_2, \theta_{12})]^2}{2\dot{\sigma}^2(r_1, r_2, \theta_{12})}\right\} \end{aligned} \tag{3.11}$$

where $\dot{m}(r_1, r_2, \theta_{12})$, $\dot{\sigma}^2(r_1, r_2, \theta_{12})$ can be obtained in the following.

From (3.1), the derivative of R_i with respect to time can be written as

$$\dot{R}_i = \sqrt{\Omega_i}\mathrm{Re}\left[\dot{S}_i\, e^{-j\Theta_i}\right] \tag{3.12}$$

where Re[·] denotes real part. The expectation of $\dot{R}_i$ conditioned on $\mathbf{S} = [S_1,\ S_2]$ is given by [16]

$$\mathbb{E}\left[\dot{R}_i|\mathbf{S}\right] = \sqrt{\Omega_i}\mathrm{Re}\left[\mathbb{E}[\dot{S}_i|\mathbf{S}]\, e^{-j\Theta_i}\right]. \tag{3.13}$$

Then one has

$$\mathbb{E}\left[\dot{Z}|\mathbf{S}\right] = \mathbb{E}\left[\dot{R}_1|\mathbf{S}\right] - \mathbb{E}\left[\dot{R}_2|\mathbf{S}\right]. \tag{3.14}$$

Combining (3.13) and (B-4) with (3.14) and after some algebraic manipulations yields

$$\begin{aligned}\dot{m}(r_1, r_2, \theta_{12}) =& \mathbb{E}\left[\dot{Z}|\mathbf{S}\right] \\ =& \frac{(r_1 + r_2)\mathrm{Re}[\dot{\rho}_{12}^{*}\rho_{12}]}{1 - |\rho_{12}|^2} \\ & - \frac{(\sqrt{\Omega_2/\Omega_1}r_1 + \sqrt{\Omega_1/\Omega_2}r_2)\mathrm{Re}[\dot{\rho}_{12}^{*}e^{j\theta_{12}}]}{1 - |\rho_{12}|^2}\end{aligned} \tag{3.15}$$

The conditional variance and covariance of $\dot{R}_1$ and $\dot{R}_2$ can be obtained as

$$\begin{aligned}&\mathrm{Var}\left[\dot{R}_i|\mathbf{S}\right] = \Omega_i \mathrm{Var}\left[\dot{S}_i|\mathbf{S}\right] \\ &\mathrm{Cov}\left[\dot{R}_1, \dot{R}_2\middle|\mathbf{S}\right] = \sqrt{\Omega_1\Omega_2}\mathrm{Re}\left\{\mathrm{Cov}\left[\dot{S}_1, \dot{S}_2\middle|\mathbf{S}\right]^{*} \mathrm{e}^{j\theta_{12}}\right\}.\end{aligned} \tag{3.16}$$

It follows that

$$\begin{aligned}\mathrm{Var}\left[\dot{R}_1 - \dot{R}_2\middle|\mathbf{S}\right] &= \mathrm{Var}\left[\dot{R}_1|\mathbf{S}\right] + \mathrm{Var}\left[\dot{R}_2|\mathbf{S}\right] - 2\mathrm{Cov}\left[\dot{R}_1, \dot{R}_2\middle|\mathbf{S}\right] \\ &= \Omega_1 \mathrm{Var}\left[\dot{S}_1|\mathbf{S}\right] + \Omega_2 \mathrm{Var}\left[\dot{S}_2|\mathbf{S}\right] \\ &\quad - 2\sqrt{\Omega_1\Omega_2}\mathrm{Re}\left\{\mathrm{Cov}\left[\dot{S}_1, \dot{S}_2\middle|\mathbf{S}\right]^{*} \mathrm{e}^{j\theta_{12}}\right\}.\end{aligned} \tag{3.17}$$

Combining (B-3) with (3.17) yields

$$\begin{aligned}\dot{\sigma}^2(r_1, r_2, \theta_{12}) &= \mathrm{Var}\left[\dot{R}_1 - \dot{R}_2\middle|\mathbf{S}\right] \\ &= -\frac{\Omega_1 + \Omega_2}{2}\left(\ddot{\rho}_{11} + \frac{|\dot{\rho}_{12}|^2}{1 - |\rho_{12}|^2}\right) \\ &\quad + \sqrt{\Omega_1\Omega_2}\mathrm{Re}\left[\left(\ddot{\rho}_{12} + \frac{\rho_{12}^{*}(\dot{\rho}_{12})^2}{1 - |\rho_{12}|^2}\right)^{*} e^{j\theta_{12}}\right].\end{aligned} \tag{3.18}$$

Then

$$\int_0^\infty \dot{z} f(\dot{z}|r_1, r_2 = r_1, \theta_{12}) \mathrm{d}\dot{z} = \frac{\dot{\sigma}(r_1, r_2 = r_1, \theta_{12})}{\sqrt{2\pi}} \exp\left[-\frac{\dot{m}^2(r_1, r_2 = r_1, \theta_{12})}{2\dot{\sigma}^2(r_1, r_2 = r_1, \theta_{12})}\right] + \frac{\dot{m}(r_1, r_2 = r_1, \theta_{12})}{2} \mathrm{erfc}\left[-\frac{\dot{m}(r_1, r_2 = r_1, \theta_{12})}{\sqrt{2}\dot{\sigma}(r_1, r_2 = r_1, \theta_{12})}\right] \quad (3.19)$$

where (3.19) is obtained using [4, eq. (3.462.5)] and erfc$(\cdot)$ is the complementary error function [4, p. 888]. Combining (3.10), (3.11) with (3.9) yields an exact expression for the switching rate.

Considering the case $\rho_{12} = \dot{\rho}_{12} = \ddot{\rho}_{12} = 0$, the two Rayleigh fading channels become independent. Then (3.9) can be simplified as

$$R_{SW}^{sc} = \frac{\sqrt{2\Omega_1\Omega_2}}{(\Omega_1 + \Omega_2)} \pi f_D. \quad (3.20)$$

When $\Omega_1 = \Omega_2$, the two branches are independent and identically distributed. Otherwise, the two branches are independent and non-identically distributed. The switching rates given by (3.20) for dual selection diversity for both i.i.d. and i.n.d. cases agree with results previously reported in [10].

3.2 Dual Correlated Rician Fading Channels

3.2.1 System Model

In a noise-free Rician fading channel, the received complex signal envelope at the i^{th} antenna is modeled as [17]

$$S_i(t) = R_i(t) e^{j\Theta_i(t)} = X_i(t) + jY_i(t) \quad (3.21)$$

where

$$X_i = R_i \cos\Theta_i$$

and

$$Y_i = R_i \sin\Theta_i$$

are independent Gaussian Random Variables (RVs) and X_1, X_2, Y_1 and Y_2 are jointly Gaussian RVs with

$$\mathbb{E}[X_i] = m_{X_i}, \quad \mathbb{E}[Y_i] = m_{Y_i}$$

and

$$\mathrm{Var}[X_i] = \mathrm{Var}[Y_i] = \sigma_i^2.$$

Then $R_i(t)$ has a Rician distribution with Rice factor

$$K_i = \frac{m_{X_i}^2 + m_{Y_i}^2}{2\sigma_i^2}.$$

3.2.2 Derivation of Analytical Expressions for Switching Rate

The JPDF of R_1, R_2, Θ_1 and Θ_2 is given by [17]

$$f_{R_1R_2\Theta_1\Theta_2}(r_1, r_2, \theta_1, \theta_2) = \frac{r_1 r_2}{(2\pi)^2\sqrt{\det(\mathbf{b})}} \exp\left[-\frac{(\mathbf{r}-\mathbf{m})^T \mathbf{b}^{-1}(\mathbf{r}-\mathbf{m})}{2}\right] \tag{3.22}$$

where $\mathbf{r} = [r_1\cos\theta_1 \; r_1\sin\theta_1 \; r_2\cos\theta_2 \; r_2\sin\theta_2]^T$, and mean vector $\mathbf{m}$ and covariance matrix $\mathbf{b}$ are given in Appendix C.

The corresponding PDF of $f(\dot{z}|r_1, r_2, \theta_1, \theta_2)$ is given by [17]

$$f_{\dot{Z}|R_1R_2\Theta_1\Theta_2}(\dot{z}|r_1, r_2, \theta_1, \theta_2) = \frac{1}{\sqrt{2\pi\dot{\sigma}^2(\mathbf{r})}} \times \exp\left\{-\frac{[\dot{z} - \dot{m}(\mathbf{r})]^2}{2\dot{\sigma}^2(\mathbf{r})}\right\} \tag{3.23}$$

where $\mathbf{R} \triangleq [R_1\cos\Theta_1 \; R_1\sin\Theta_1 \; R_2\cos\Theta_2 \; R_2\sin\Theta_2]^T$, $\dot{m}(\mathbf{R}) = \mathbb{E}[\dot{Z}|\mathbf{R}]$ and $\dot{\sigma}^2(\mathbf{R}) = \mathrm{Var}[\dot{Z}|\mathbf{R}]$ can be obtained by

$$\dot{m}(\mathbf{R}) = \dot{m}_1(\mathbf{R}) - \dot{m}_2(\mathbf{R}) \tag{3.24a}$$

$$\dot{\sigma}^2(\mathbf{R}) = \dot{\sigma}_1^2(\mathbf{R}) + \dot{\sigma}_2^2(\mathbf{R}) - 2\dot{\sigma}_{12}^2(\mathbf{R}) \tag{3.24b}$$

where $\dot{m}_i(\mathbf{R})$, $\dot{\sigma}_i^2(\mathbf{R})$ and $\dot{\sigma}_{ij}^2(\mathbf{R})$ are given in [17, (6a)-(6c)]

$$\dot{m}_i(\mathbf{R}) = \mathbb{E}\left[\dot{X}_i|\mathbf{R}\right]\cos\Theta_i + \mathbb{E}\left[\dot{Y}_i|\mathbf{R}\right]\sin\Theta_i \tag{3.25a}$$

$$\begin{aligned}\dot{\sigma}_i^2(\mathbf{R}) =& \mathrm{Var}\left[\dot{X}_i|\mathbf{R}\right]\cos^2\Theta_i + \mathrm{Var}\left[\dot{Y}_i|\mathbf{R}\right]\sin^2\Theta_i \\ &+ \mathrm{Cov}\{\dot{X}_i, \dot{Y}_i|\mathbf{R}\}\sin 2\Theta_i\end{aligned} \tag{3.25b}$$

$$\begin{aligned}\dot{\sigma}_{ij}^2(\mathbf{R}) =& \mathrm{Cov}\{\dot{X}_i, \dot{X}_j|\mathbf{R}\}\cos\Theta_i\cos\Theta_j + \mathrm{Cov}\{\dot{X}_i, \dot{Y}_j|\mathbf{R}\}\cos\Theta_i\sin\Theta_j \\ &+ \mathrm{Cov}\{\dot{Y}_i, \dot{X}_j|\mathbf{R}\}\sin\Theta_i\cos\Theta_j + \mathrm{Cov}\{\dot{Y}_i, \dot{Y}_j|\mathbf{R}\}\sin\Theta_i\sin\Theta_j.\end{aligned} \tag{3.25c}$$

Combining the results in Appendix C with (3.25), one can get the quantities $\dot{\sigma}^2(\mathbf{R})$ and $\dot{m}(\mathbf{R})$.

Then the exact expression for the switching rate is

$$R_{SW}^{sc} = 2\int_0^{2\pi}\int_0^{2\pi}\int_0^{\infty} R_+(r_1, r_2 = r_1, \theta_1, \theta_2) f(r_1, r_2 = r_1, \theta_1, \theta_2)\mathrm{d}r_1\mathrm{d}\theta_1\mathrm{d}\theta_2 \tag{3.26}$$

where

$$\begin{aligned}R_+(r_1, r_2 = r_1, \theta_1, \theta_2) &= \int_0^{\infty} \dot{z} f(\dot{z}|r_1, r_2 = r_1, \theta_1, \theta_2)\mathrm{d}\dot{z} \\ &= \frac{\dot{\sigma}(r_1, r_2 = r_1, \theta_1, \theta_2)}{\sqrt{2\pi}}\exp\left[-\frac{\dot{m}^2(r_1, r_2 = r_1, \theta_1, \theta_2)}{2\dot{\sigma}^2(r_1, r_2 = r_1, \theta_1, \theta_2)}\right] \\ &+ \frac{\dot{m}(r_1, r_2 = r_1, \theta_1, \theta_2)}{2}\mathrm{erfc}\left[-\frac{\dot{m}(r_1, r_2 = r_1, \theta_1, \theta_2)}{\sqrt{2}\dot{\sigma}(r_1, r_2 = r_1, \theta_1, \theta_2)}\right].\end{aligned} \tag{3.27}$$

Considering the case $\rho_{12} = \dot{\rho}_{12} = \ddot{\rho}_{12} = 0$, (3.26) yields the same results given in [10, Table I] for Rician fading, as required.

3.3 Numerical Results

Numerical examples are presented for a space diversity system with horizontally spaced omnidirectional antennas at the mobile station under a 2-*D* isotropic scattering environment

[16]

$$\rho_{11}(\tau) = J_0(2\pi f_D \tau) \tag{3.28}$$

$$\rho_{12}(\tau) = J_0\left(2\pi\sqrt{(f_D\tau)^2 + \left(\frac{d}{\lambda}\right)^2 - 2f_D\tau\frac{d}{\lambda}\cos\alpha}\right) \tag{3.29}$$

$$\ddot{\rho}_{11} = -2(\pi f_D)^2 \tag{3.30}$$

$$\rho_{12} = J_0\left(2\pi\frac{d}{\lambda}\right) \tag{3.31}$$

$$\dot{\rho}_{12} = 2\pi f_D J_1\left(2\pi\frac{d}{\lambda}\right)\cos\alpha \tag{3.32}$$

$$\ddot{\rho}_{12} = (2\pi f_D)^2\left[\frac{J_1(2\pi\frac{d}{\lambda})}{2\pi\frac{d}{\lambda}}\cos 2\alpha - J_0\left(2\pi\frac{d}{\lambda}\right)\cos^2\alpha\right] \tag{3.33}$$

where $J_n(\cdot)$ is the n^{th} order Bessel function of the first kind, d is the antenna spacing, λ is the carrier wavelength, and $0 \leq \alpha \leq \frac{\pi}{2}$ is the angle between the antenna axis and the direction of vehicle motion. The antenna configuration is illustrated in Fig. 3.1.

In the numerical results, the switching rate is normalized by the Doppler frequency and we define $c_\sigma = \sigma_2/\sigma_1$. Overall, Figs. 3.2 - 3.7 show that the switching rate for correlated dual diversity branches can be either greater or lesser than that for the case of independent diversity branches, depending on the angle α and the antenna spacing. It is observed that the switching rate of dual correlated branches converges to the switching rate of dual independent branches as $\frac{d}{\lambda} \to \infty$, as expected.

Fig. 3.2 gives a comparison of normalized switching rates of dual selection combining for balanced correlated Rayleigh fading diversity branches for different values of the antenna angle, α, with the normalized switching rate of dual i.i.d. fading. Fig. 3.3 shows a comparison of normalized switching rates of dual selection combining for unbalanced correlated Rayleigh fading diversity branches for different values of α with dual i.n.d. fading. Comparing the results in Fig. 3.3 with those in Fig. 3.2, one sees that a large unbalance

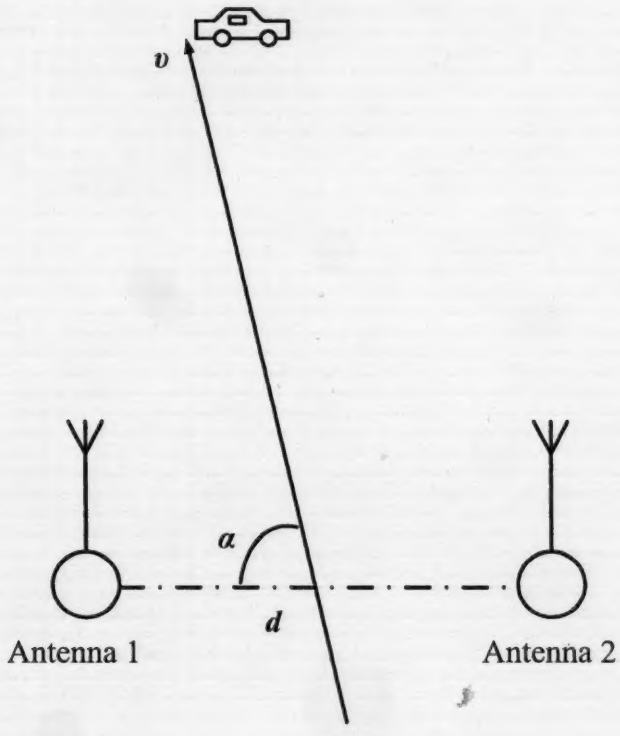

Fig. 3.1. The antenna configuration.

between the antennas causes the switching rate to be smaller; this is true for both the independent case and the correlated case because the antenna with the greater power becomes preferred. Furthermore, the switching rate for $\alpha = \frac{\pi}{2}$ is close to the switching rate for independent diversity branches and the antennas appear more "uncorrelated" because they are not in the same direction. Fig. 3.3 further indicates that in the case of large unbalance, with correlated diversity branches, the switching rates also vacillate around the switching rate for independent diversity branches.

For correlated Rician fading scenarios, the normalized switching rates are affected by

the antenna angle, α, the antenna spacing, the Rice factors, K_i, and the scatter powers, σ_i. For simplicity, one considers the case $m_{Y_1} = m_{Y_2} = 0$. Fig. 3.4 gives a comparison of normalized switching rates of dual selection combining for balanced correlated Rician fading branches with different values of the antenna angle, α, and dual i.i.d. fading. As the Rice factor K_i increases, the normalized switching rate decreases. Fig. 3.5 gives a comparison of normalized switching rates of dual selection combining for correlated Rician fading branches with equal Rice factors for different values of the antenna angle, α, and dual independent fading. One sees that a large unbalance between the antennas leads the switching rate to be smaller because the antenna with the greater power is preferred for both independent and correlated fadings. Fig. 3.6 shows a comparison of normalized switching rates of dual selection combining for correlated Rician fading branches with equal scatter powers for different values of the antenna angle, α, and dual independent fading. The normalized switching rates have large vacillations for correlated Rician fading. Fig. 3.7 shows a comparison of normalized switching rates of dual selection combining for correlated Rician fading branches with unequal scatter powers and unequal Rice factors for different values of the antenna angle, α, and dual independent fading. The switching rate for $\alpha = \frac{\pi}{2}$ is generally closest to the switching rate for independent diversity branches.

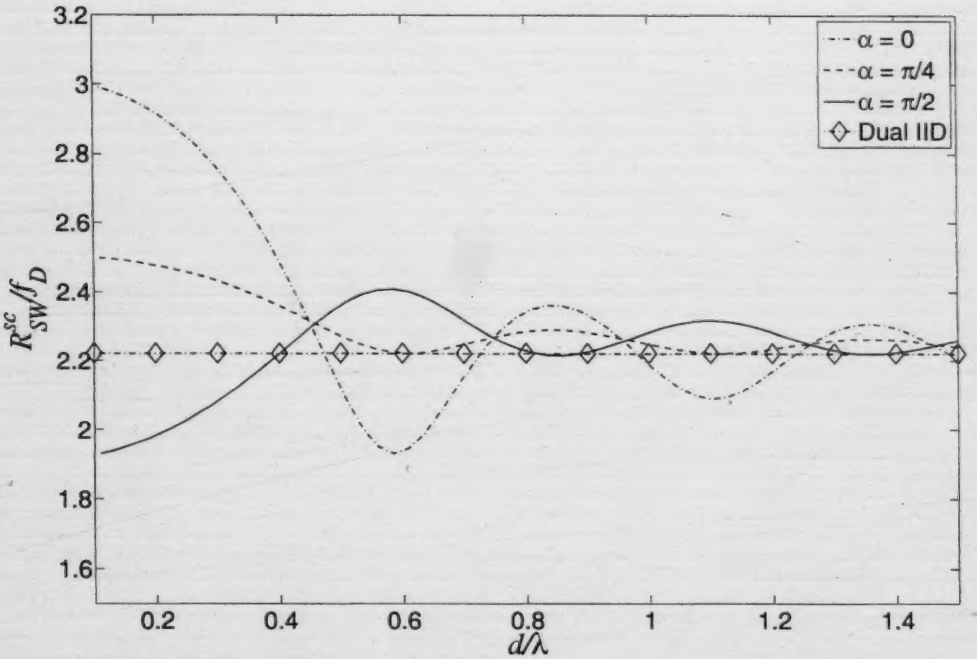

Fig. 3.2. Comparison of normalized switching rates of dual selection combining for balanced correlated Rayleigh fading branches with different values of the antenna angle, α, and dual i.i.d. fading ($\Omega_1 = \Omega_2 = 0.5$).

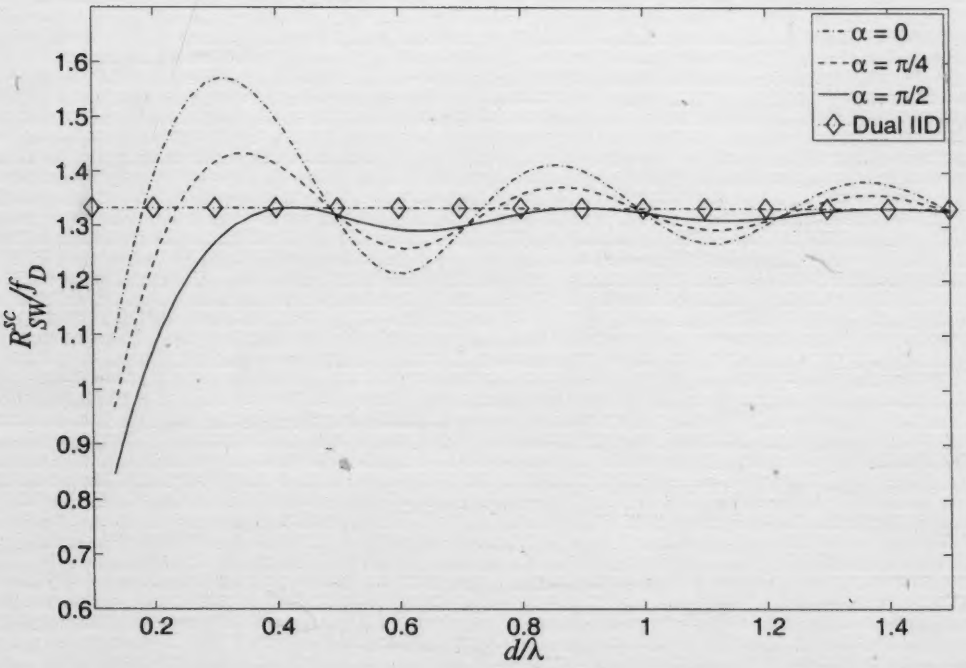

Fig. 3.3. Comparison of normalized switching rates of dual selection combining for unbalanced correlated Rayleigh fading branches with different values of the antenna angle, α, and dual i.n.d. fading ($\Omega_1 = 0.1, \Omega_2 = 0.9$).

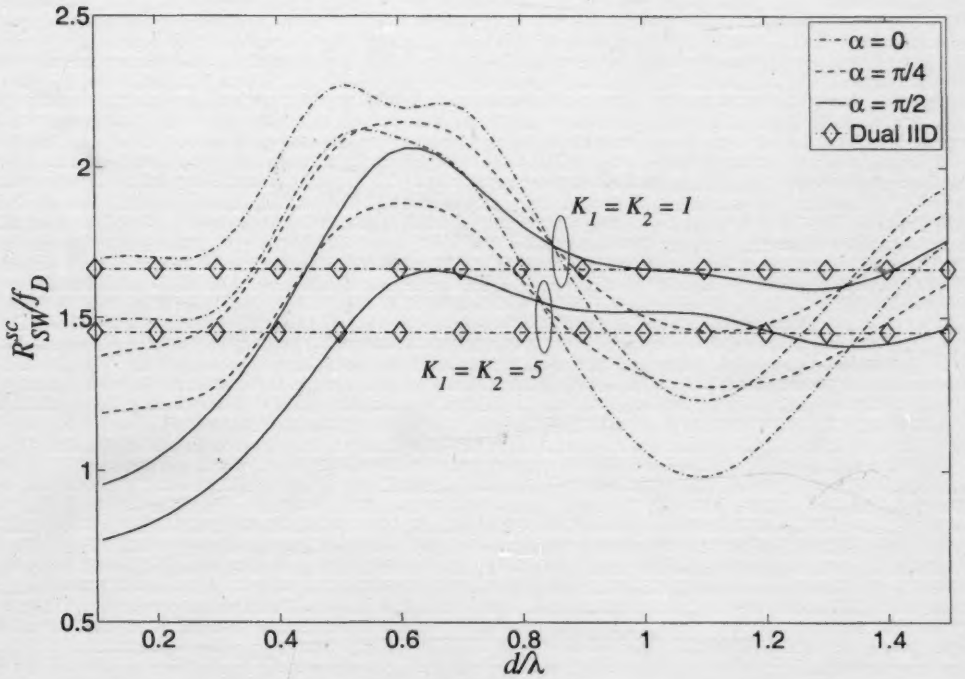

Fig. 3.4. Comparison of normalized switching rates of dual selection combining for balanced correlated Rician fading branches with different values of the antenna angle, α, and dual i.i.d. fading ($\sigma_1 = \sigma_2$).

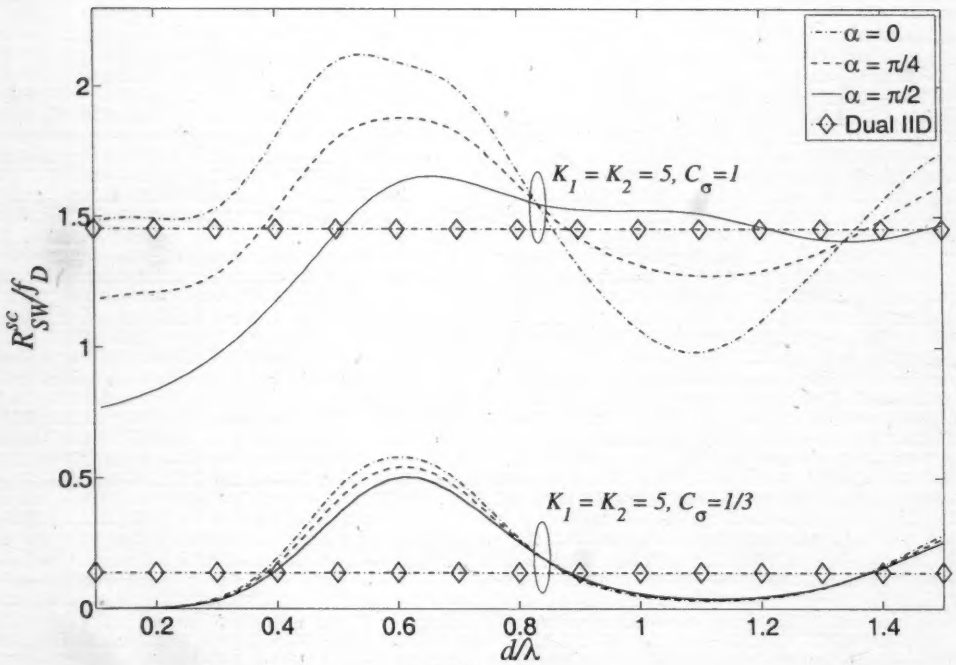

Fig. 3.5. Comparison of normalized switching rates of dual selection combining for correlated Rician fading branches with equal Rice factors for different values of the antenna angle, α, and dual independent fading.

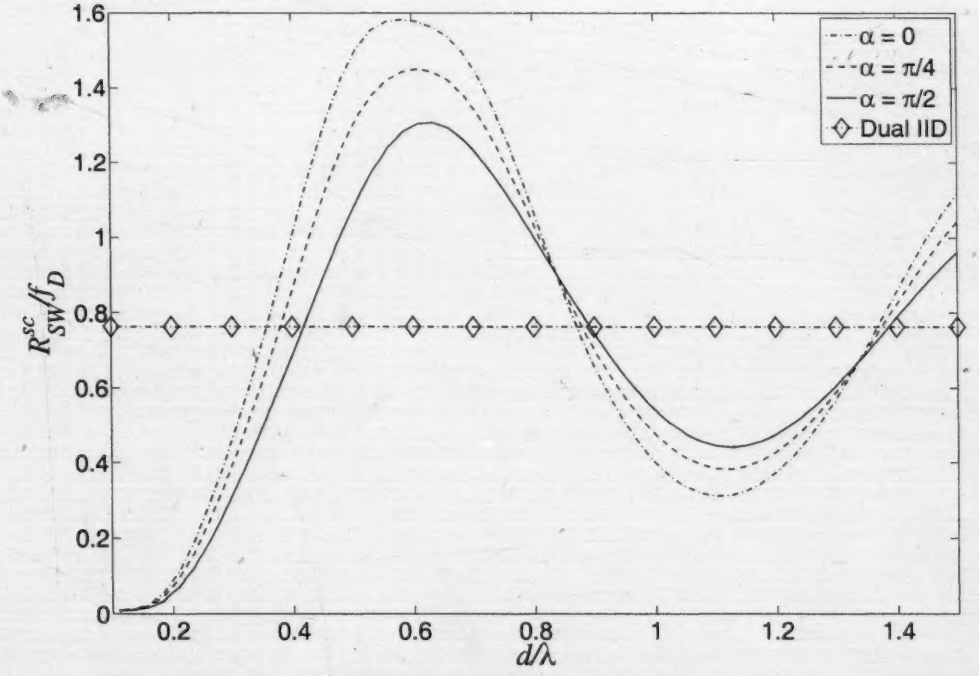

Fig. 3.6. Comparison of normalized switching rates of dual selection combining for correlated Rician fading branches with equal scatter powers for different values of the antenna angle, α, and dual independent fading ($K_1 = 1$, $K_2 = 5$, $\sigma_1 = \sigma_2$).

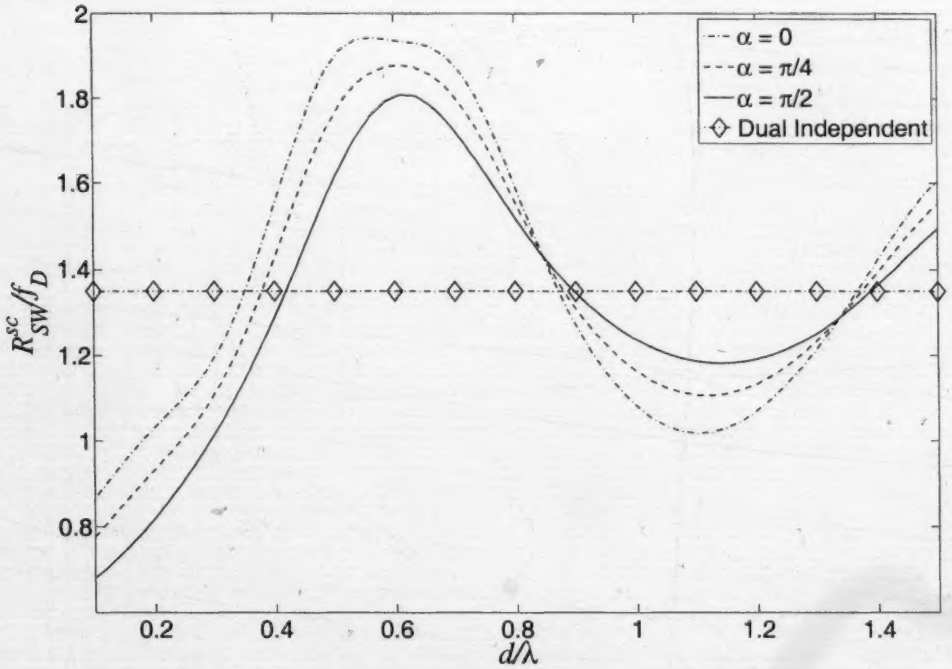

Fig. 3.7. Comparison of normalized switching rates of dual selection combining for correlated Rician fading branches with unequal scatter powers and unequal Rice factors for different values of the antenna angle, α, and dual independent fading ($K_1 = 1$, $K_2 = 5$, $c_\sigma = 1/3$).

Chapter 4

Switching Rates of Two-Branch Selection Diversity in κ-μ and α-μ Distributed Fading

The κ-μ distribution proposed by [5] provides a better fit to field measurements than Rician and Nakagami-m and it describes the small scale variation of a fading signal with the existence of a LOS path. When $\mu = 1$, the κ-μ distribution becomes the Rician distribution with κ as the Rice factor. Furthermore, if $\kappa = 0$, the κ-μ distribution is equivalent to the Rayleigh distribution [6]. Reference [5] has shown that the κ-μ distribution is exactly the same as the Nakagami-m distribution as $\kappa \to 0$. Moreover, the κ-μ distribution fully describes the characteristics of the fading signal in terms of measurable physical parameters.

The α-μ distribution is considering non-linearity of the propagation medium and clusters of multipath waves, which also provides a good fit to field measurement data [7]. By setting $\alpha = 2$, the α-μ distribution is specialized to the Nakagami-m distribution. Furthermore, by setting $\mu = 1$, the Rayleigh distribution is obtained.

References [6] examined the level crossing rate and average fade duration of the κ-μ

fading signal, while [8] examined the level crossing rate and fade durations for diversity systems of the α-μ fading channels. Both, however, did not study the switching rate of selection diversity combining. In this chapter, an analytical expression for the switching rate is derived for dual selection diversity combining. Dual i.i.d. κ-μ and α-μ fading channels are adopted, and numerical results are presented.

4.1 Dual κ-μ Fading Channels

The definition of conditional probability density function is given by [18]

$$f_{Z\dot{Z}}(z,\dot{z}) = f_{\dot{Z}|Z}(\dot{z}|z) f_Z(z). \tag{4.1}$$

One can simplify (2.9) using (4.1)

$$R_{SW}^{sc} = 2 f_Z(0) \int_0^\infty \dot{z} f_{\dot{Z}|Z}(\dot{z}|z=0) \mathrm{d}\dot{z}. \tag{4.2}$$

Reference [6] has shown that the fading envelope $R_i(t)$ is independent of derivative process $\dot{R}_i(t)$. It follows that the fading processes $Z(t)$ and $\dot{Z}(t)$ are also independent, that is, $f(\dot{z}|z) = f(\dot{z})$ and (4.2) specializes to

$$R_{SW}^{sc} = 2 f_Z(0) \int_0^\infty \dot{z} f_{\dot{Z}}(\dot{z}) \mathrm{d}\dot{z}. \tag{4.3}$$

In order to evaluate (4.3), $f_Z(z=0)$ is required. Define the two-dimensional transformation

$$Z = R_1 - R_2 \tag{4.4a}$$

$$R_1 = R_1. \tag{4.4b}$$

The Jacobian of (4.4) is $\mathbf{J} = 1$. Using the fact that R_1 and R_2 are independent gives

$$f_{ZR_1}(z, r_1) = f_{R_1R_2}(r_1, r_1 - z) = f_{R_1}(r_1) f_{R_2}(r_1 - z). \tag{4.5}$$

Then one has

$$f_Z(0) = \int_0^\infty f_{ZR_1}(z=0, r_1)\mathrm{d}r_1$$
$$= \int_0^\infty f_{R_1}(r_1) f_{R_2}(r_1)\mathrm{d}r_1. \tag{4.6}$$

When the two fading branches are i.i.d., (4.6) specializes to

$$f_Z(0) = \int_0^\infty [f_R(r)]^2 \mathrm{d}r. \tag{4.7}$$

Using the relation [4, (8.406.1)]

$$I_n(z) = j^{-n} J_n(jz), \tag{4.8}$$

(1.20) can be written as

$$f_R(r) = \frac{2\mu(1+\kappa)^{\frac{\mu+1}{2}}}{\hat{r}\kappa^{\frac{\mu-1}{2}}\exp(\mu\kappa)} \left(\frac{r}{\hat{r}}\right)^{\mu}$$
$$\times \exp\left[-\mu(1+\kappa)\left(\frac{r}{\hat{r}}\right)^2\right] j^{-\mu+1} J_{\mu-1}\left[j2\mu\sqrt{\kappa(1+\kappa)}\frac{r}{\hat{r}}\right]. \tag{4.9}$$

Substituting (4.9) into (4.7) yields the quantity $f_Z(0)$

$$f_Z(0) = \int_0^\infty \frac{4\mu^2(1+\kappa)^{\mu+1}}{\hat{r}^2\kappa^{\mu-1}\exp(2\mu\kappa)} \left(\frac{r}{\hat{r}}\right)^{2\mu}$$
$$\times \exp\left[-2\mu(1+\kappa)\left(\frac{r}{\hat{r}}\right)^2\right] j^{-2\mu+2} J_{\mu-1}^2\left[j2\mu\sqrt{\kappa(1+\kappa)}\frac{r}{\hat{r}}\right]\mathrm{d}r$$
$$= \frac{2^{3/2-2\mu}\sqrt{\mu(1+\kappa)}}{\hat{r}\exp(2\mu\kappa)} \frac{\Gamma(2\mu-1/2)}{\Gamma^2(\mu)}$$
$$\times {}_3F_3\left(\mu-\frac{1}{2}, \mu, 2\mu-\frac{1}{2}; \mu, \mu, 2\mu-1; 2\mu\kappa\right) \tag{4.10}$$

where [4, (6.633.5)] is used to obtain the integral result and the integration requires $\mu > \frac{1}{4}$; otherwise the integral (4.10) can be evaluated by numerical integration. The expression for

${}_3F_3\left(\mu-\frac{1}{2},\mu,2\mu-\frac{1}{2};\mu,\mu,2\mu-1;2\mu\kappa\right)$ can be simplified using [4, (9.14.1)]

$$\begin{aligned}
&{}_3F_3\left(\mu-\frac{1}{2},\mu,2\mu-\frac{1}{2};\mu,\mu,2\mu-1;2\mu\kappa\right)\\
&=\sum_{k=0}^{\infty}\frac{(\mu-\frac{1}{2})_k(\mu)_k(2\mu-\frac{1}{2})_k}{(\mu)_k(\mu)_k(2\mu-1)_k}\frac{(2\mu\kappa)^k}{k!}\\
&=\sum_{k=0}^{\infty}\frac{(\mu-\frac{1}{2})_k(2\mu-\frac{1}{2})_k}{(\mu)_k(2\mu-1)_k}\frac{(2\mu\kappa)^k}{k!}\\
&={}_2F_2\left(\mu-\frac{1}{2},2\mu-\frac{1}{2};\mu,2\mu-1;2\mu\kappa\right) \qquad (4.11)
\end{aligned}$$

where

$$(\alpha)_k=\alpha(\alpha+1)\cdots(\alpha+k-1)=\frac{\Gamma(\alpha+k)}{\Gamma(\alpha)}$$

is the Pochhammer symbol [4]. Now, (4.10) can be written as

$$\begin{aligned}
f_Z(0)=&\frac{2^{3/2-2\mu}\sqrt{\mu(1+\kappa)}}{\hat{r}\exp(2\mu\kappa)}\frac{\Gamma(2\mu-1/2)}{\Gamma^2(\mu)}\\
&\times {}_2F_2\left(\mu-\frac{1}{2},2\mu-\frac{1}{2};\mu,2\mu-1;2\mu\kappa\right). \qquad (4.12)
\end{aligned}$$

The integral in (4.3) is given by [6]

$$\begin{aligned}
\int_0^{\infty}\dot{z}f_{\dot{Z}}(\dot{z})\mathrm{d}\dot{z}&=\int_0^{\infty}\frac{\dot{z}}{\sqrt{2\pi}\sigma_{\dot{Z}}}\exp\left(-\frac{(\dot{z})^2}{2\sigma_{\dot{Z}}^2}\right)\mathrm{d}\dot{z}\\
&=\frac{\sigma_{\dot{Z}}}{\sqrt{2\pi}} \qquad (4.13)
\end{aligned}$$

where [4, 3.461.3] is used and $\sigma_{\dot{Z}}$ is given by [6]

$$\sigma_{\dot{Z}}^2=2\sigma_{\dot{R}}^2=4\pi^2\sigma^2f_D^2.$$

Combining (4.12) and (4.13) with (4.7) yields an analytical expression for the switching rate normalized by the maximum Doppler frequency

$$\begin{aligned}
R_{SW}^{sc}/f_D=&2^{2(1-\mu)}\sqrt{2\pi}\exp(-2\mu\kappa)\frac{\Gamma(2\mu-1/2)}{\Gamma^2(\mu)}\\
&\times {}_2F_2\left(\mu-\frac{1}{2},2\mu-\frac{1}{2};\mu,2\mu-1;2\mu\kappa\right). \qquad (4.14)
\end{aligned}$$

Considering $\mu = 1$, and replacing κ with the Rice factor K, one can simplify (4.14) to obtain the normalized switching rate for dual i.i.d. Rician fading channels as

$$R_{SW}^{sc}/f_D = \frac{\pi}{\sqrt{2}}\exp(-2K)\ {}_2F_2\left(\frac{1}{2},\frac{3}{2};1,1;2K\right). \tag{4.15}$$

Eq. (4.15) agrees with the result given in [10, Table I]. Setting $K = 0$ and using the fact, ${}_2F_2(\cdot,\cdot;\cdot,\cdot;0) = 1$, yields the normalized switching rate for dual i.i.d. Rayleigh fading channels as

$$R_{SW}^{sc}/f_D = \frac{\pi}{\sqrt{2}}. \tag{4.16}$$

Eq. (4.16) agrees with the result given in [10, Table I]. As $\kappa \to 0$, replacing μ with Nakagami parameter, m, one can write (4.14) as

$$R_{SW}^{sc}/f_D = \sqrt{\pi}2^{\frac{5}{2}-2m}\frac{\Gamma\left(2m-\frac{1}{2}\right)}{\Gamma^2(m)}. \tag{4.17}$$

Eq. (4.17) is the normalized switching rate for dual i.i.d. Nakagami-m fading channels and it agrees with the result given in [10, Table I]. Note that $\mu > \frac{1}{4}$ is required to validate (4.14), which is satisfied by $m \geq \frac{1}{2}$ [10]. While (4.15), (4.16) and (4.17) have been reported in [10], (4.14) is a new unifying result that is more general than previous results and includes them as special cases.

4.2 Dual α-μ Fading Channels

In this section, we will derive the closed-form expression for the switching rate of selection diversity combining in dual α-μ fading channels. Eq. (2.9) can be written as

$$R_{SW}^{sc} = 2\int_0^\infty \int_0^\infty \dot{z} f_{Z\dot{Z}R_1}(0,\dot{z},r_1)\mathrm{d}r_1\mathrm{d}\dot{z}. \tag{4.18}$$

Combining the identity $f_{\dot{Z}R_1R_2}(\dot{z},r_1,r_2) = f_{\dot{Z}|R_1R_2}(\dot{z}|r_1,r_2)f_{R_1R_2}(r_1,r_2)$ and the fact $Z = R_1 - R_2 = 0$ with (4.18) yields

$$R_{SW}^{sc} = 2\int_0^\infty \int_0^\infty \dot{z} f_{\dot{Z}|R_1R_2}(\dot{z}|r_1,r_2 = r_1)f_{R_1R_2}(r_1,r_2 = r_1)\mathrm{d}r_1\mathrm{d}\dot{z}. \tag{4.19}$$

One has the expression for $f_{\dot{Z}|R_1R_2}(\dot{z}|r_1, r_2 = r_1)$ given at [8]

$$f_{\dot{Z}|R_1R_2}(\dot{z}|r_1, r_2 = r_1) = \frac{1}{\sqrt{2\pi}\sigma_{\dot{Z}}} \exp\left(-\frac{\dot{z}^2}{2\sigma_{\dot{Z}}^2}\right) \tag{4.20}$$

where

$$\sigma_{\dot{Z}}^2 = 4\pi^2 f_D^2 \left(\frac{r_1^{2-\alpha_1}}{\alpha_1^2 \mu_1}\Omega_1 + \frac{r_2^{2-\alpha_2}}{\alpha_2^2 \mu_2}\Omega_2\right)$$
$$\Omega_i = \hat{r}_i^{\alpha_i}.$$

Note that $\sigma_{\dot{Z}}$ depends on R_1 and R_2. Then (4.19) becomes

$$R_{SW}^{sc} = 2\int_0^\infty \frac{\sigma_{\dot{Z}}}{\sqrt{2\pi}} f_{R_1R_2}(r_1, r_2 = r_1)\mathrm{d}r_1. \tag{4.21}$$

Since R_1 is independent of R_2, we have

$$f_{R_1R_2}(r_1, r_2 = r_1) = f_{R_1}(r_1) f_{R_2}(r_1). \tag{4.22}$$

Here, we consider dual i.i.d. fading signals, i.e. $f_{R_1}(r_1) = f_{R_2}(r_2)$. Substituting (1.22) and (4.22) into (4.21) yields an exact normalized switching rate for dual α-μ fading signals

$$\begin{aligned} R_{SW}^{sc}/f_D &= 2\frac{\sigma_{\dot{Z}}}{\sqrt{2\pi}} \int_0^\infty \frac{\alpha^2 \mu^{2\mu} r_1^{2\alpha\mu-1}}{\hat{r}^{2\alpha\mu}\Gamma^2(\mu)} \exp\left(-\frac{2\mu r_1^\alpha}{\hat{r}^\alpha}\right) \mathrm{d}r_1 \\ &= \frac{2^{5/2-2\mu}\sqrt{\pi}}{\Gamma^2(\mu)}\Gamma\left(2\mu - \frac{1}{2}\right) \end{aligned} \tag{4.23}$$

where [4, (3.478.1)] is used to obtain the integral result and the integration requires $\mu > \frac{1}{4}$; otherwise the integral (4.21) can be evaluated by numerical integration. It is noted that (4.23) depends only on the parameter μ, and (4.23) can be obtained by setting $\kappa = 0$ in (4.14). Replacing μ with Nakagami parameter m yields

$$R_{SW}^{sc}/f_D = \frac{2^{5/2-2m}\sqrt{\pi}}{\Gamma^2(m)}\Gamma\left(2m - \frac{1}{2}\right) \tag{4.24}$$

which is the normalized switching rate for dual i.i.d. Nakagami-m fading channels in agreement with (4.17). As a second special case, one obtains (4.16) by setting $\mu = 1$ in (4.23).

4.3 Numerical Results

A closed-form expression for the switching rate of dual selection combining in dual i.i.d. general κ-μ and α-μ fading channels has been derived. Sample numerical results are presented by specializing κ and μ in the κ-μ distribution and μ in the α-μ distribution. Fig. 4.1 gives the normalized switching rates of dual selection combining in i.i.d. κ-μ fading branches with fixed values of parameter, μ. In general, the normalized switching rates decrease as the parameter, κ, increases. When $\mu = 0.5$, the normalized switching rate decreases exponentially, which is expected since ${}_2F_2(0, 0.5; 0.5, 0; \kappa) = 1$ in (4.14). When $\mu = 0.8$, 1, and 4, the normalized switching rates are almost invariant for $\kappa > 1.5$. Fig. 4.2 gives the normalized switching rates of dual selection combining in i.i.d. κ-μ fading branches with fixed values of parameter, κ. When $\kappa = 0$, the result is exactly the same as the normalized switching rate for dual i.i.d. Nakagami-*m* fading channels. When $\kappa = 1$, 2, 3, and 5, the normalized switching rates have their minima at $\mu = 0.5$, and they are invariant as μ becomes larger. Fig. 4.3 shows a comparison of theoretical and simulated normalized switching rates of dual selection combining in i.i.d. κ-μ fading branches for $\mu = 2$. There is excellent agreement between the simulation results and the theoretical results. Fig. 4.4 shows a comparison of theoretical and simulated normalized switching rates of dual selection combining in i.i.d. α-μ fading branches. As expected, the result is the same as the normalized switching rate for dual i.i.d. κ-μ fading branches with $\kappa = 0$. It again is observed that the simulation results have excellent agreement with the theoretical results.

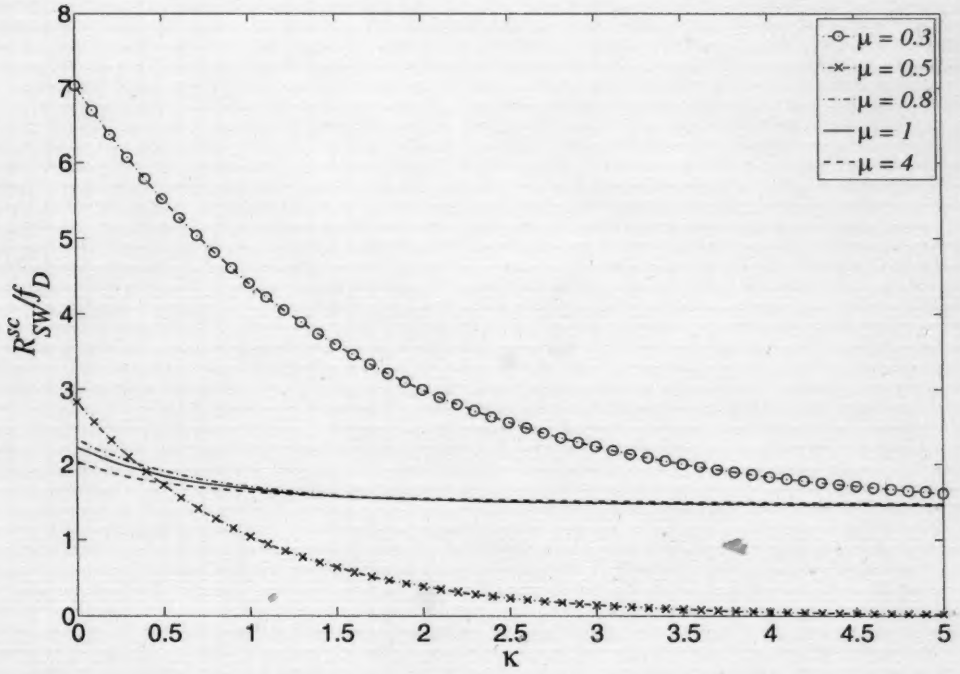

Fig. 4.1. Normalized switching rates of dual selection combining in i.i.d. κ-μ fading branches with fixed values of parameter, μ.

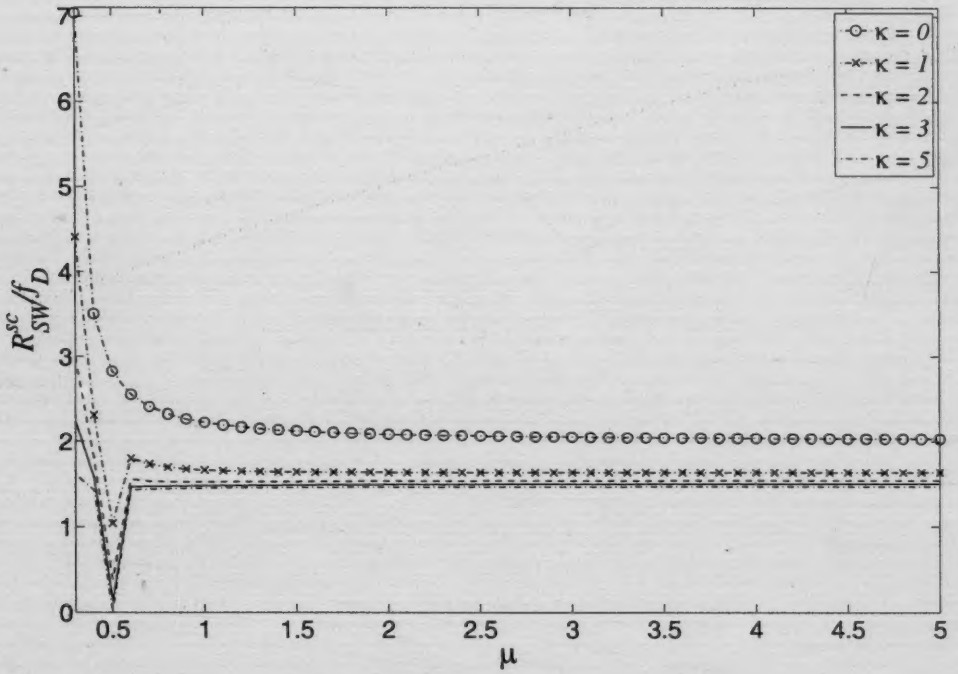

Fig. 4.2. Normalized switching rates of dual selection combining in i.i.d. κ-μ fading branches with fixed values of parameter, κ.

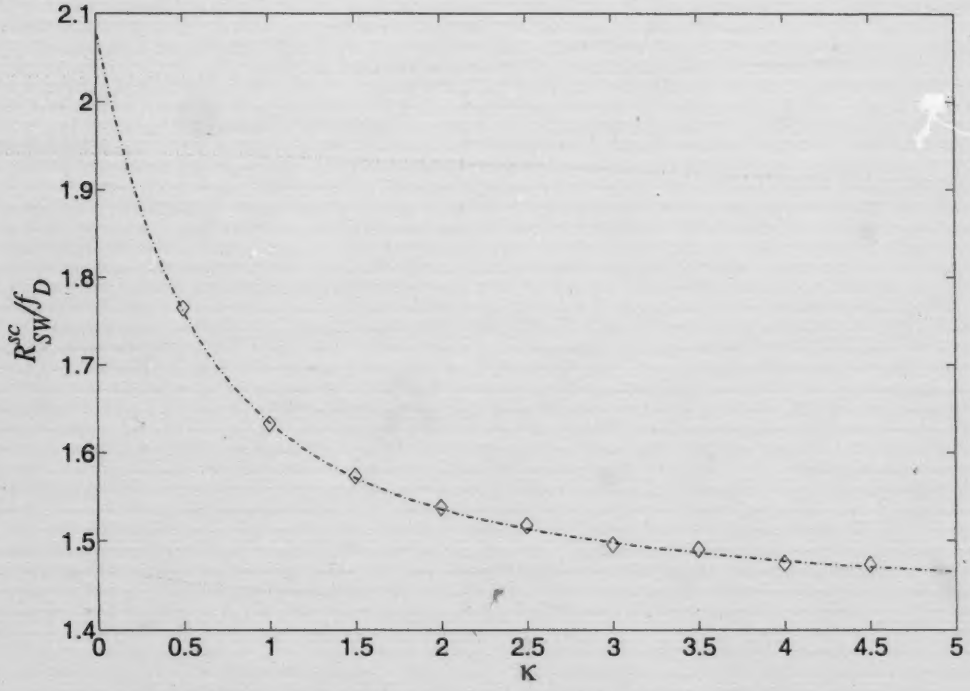

Fig. 4.3. Comparison of theoretical (dash-dotted line) and simulated (diamond) normalized switching rates of dual selection combining in i.i.d. κ-μ fading branches for $\mu = 2$.

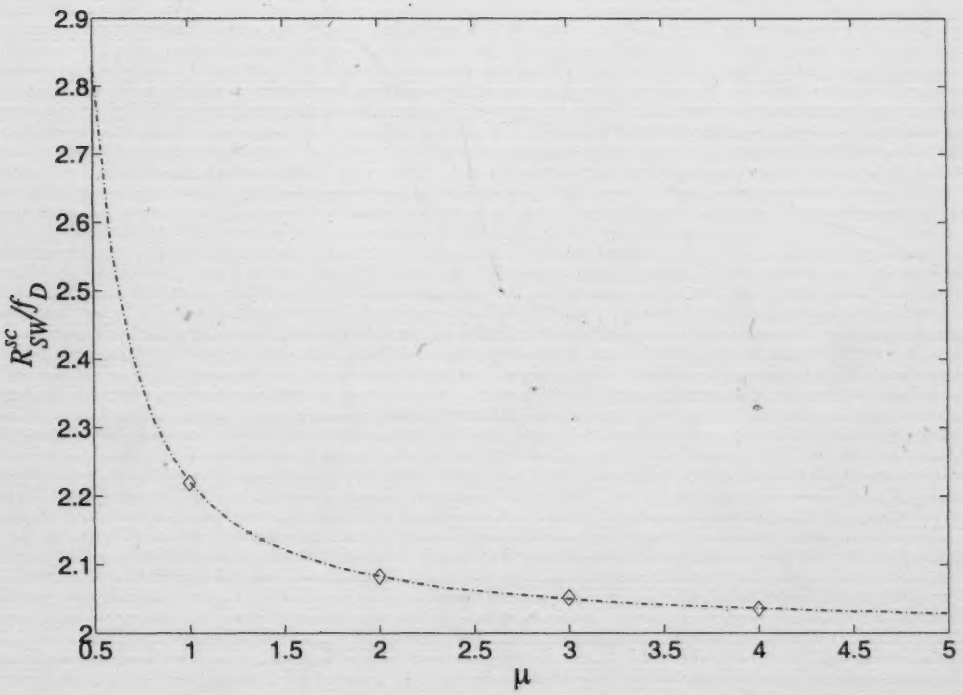

Fig. 4.4. Comparison of theoretical (dash-dotted line) and simulated (diamond) normalized switching rates of dual selection combining in i.i.d. α-μ fading branches.

Chapter 5

Switching Rates of Dual Selection Diversity in Noisy Fading Channels

So far, we have only considered fading channels in the absence of noise. In practical communication systems, the transmitted signal is contaminated with noise, which is random and unpredictable. Noise is generally divided into two categories, external noise and internal noise. External noise includes interference from nearby channels, human-made noise, automobile ignition, lightning and so on. Such noise can be minimized or even eliminated with proper techniques. On the other hand, internal noise results from the thermal motion of electrons, random emission and diffusion of charged carriers in electronic circuits. With proper techniques, the effects of internal noise can be reduced, but can never be eliminated [19].

Noise is unavoidable and it degrades the quality of signals and systems. Branch switching in selection diversity is affected by noise. Therefore, it is essential to investigate the behavior of the switching rate in noisy fading channels. Yet, no published literature examines diversity switching rate in noisy fading channels. Reference [20] examined the inphase zero crossing rate, inphase rate of maxima, phase zero crossing rate, and the in-

staneous frequency zero crossing rate of selection diversity combining in noisy Rayleigh fading channels, but did not examine the switching rate. In this paper, an analytical expression for the switching rate is derived for dual selection diversity combining in the presence of noise. Both i.i.d. and i.n.d. cases are considered, and numerical results are presented.

5.1 System Model

We consider the following system model. The received lowpass complex signal envelope at the i^{th} antenna ($i = 1,2$), $s_i(t)$, is bandlimited by a receiver filter with a bandwidth of B_w Hz greater than or equal to the maximum Doppler frequency and corrupted by additive complex noise, $n_i(t)$, to yield

$$c_i(t) = s_i(t) + n_i(t) \tag{5.1}$$

where $s_i(t)$ is a complex Gaussian random process representing channel gain, $n_i(t)$ is a zero-mean complex Gaussian random process representing additive noise and $s_i(t)$ and $n_i(t)$ are mutually independent. In the case of Rayleigh fading, s_i is zero-mean whereas in the case of Rician fading, it is non-zero mean. The noise n_i is bandlimited with bandwidth B_w Hz, and has a two-sided power spectral density of $N_o/2$ watts/Hz. The resulting total power of n_i is $N_o B_w$ watts. Note that (5.1) can be written in complex form as

$$c_i(t) = x_i(t) + jy_i(t) = r_i(t)e^{j\theta_i(t)} \tag{5.2}$$

where $x_i(t)$ and $y_i(t)$ are inphase and quadrature components, respectively and $r_i(t)$ and $\theta_i(t)$ are the envelope and the phase of $c_i(t)$, respectively. Fig. 5.1 shows the PSD of the received signal $c_i(t)$ [21].

The autocorrelation function of the received complex envelope $c_i(t)$ is defined as

$$\phi_{c_i c_i}(\tau) = \frac{1}{2}\mathbb{E}[c_i^*(t)c_i(t+\tau)]$$

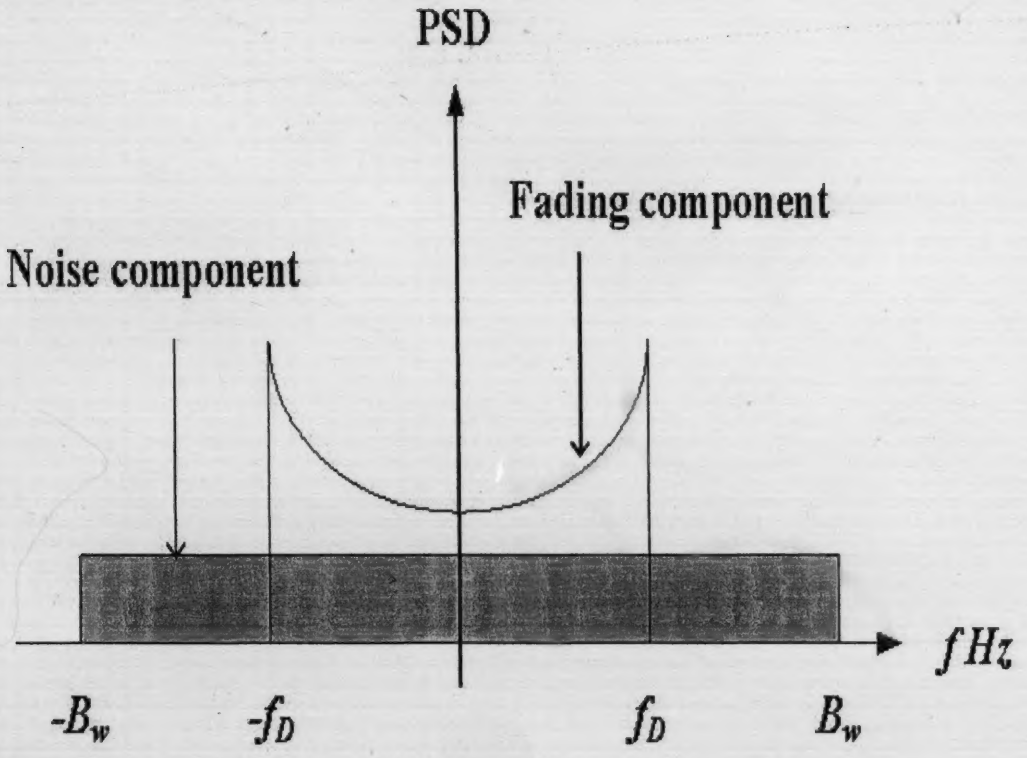

Fig. 5.1. Power spectral desity of received signal envelope and bandlimited Gaussian noise for a 2-D isotropic fading channel with an omnidirectional antenna (after [21, Fig. 1]).

and its power spectral density is given as $S_{c_ic_i}(f)$. The n^{th} spectral moment of $c_i(t)$, $b_{i,n}$, $n = 0, 1, 2, \cdots$, is given by [20, eq. (5)]

$$b_{i,n} = (2\pi)^n \int_{-\infty}^{\infty} f^n S_{c_ic_i}(f)\mathrm{d}f = \frac{\mathrm{d}^n \phi_{c_ic_i}(\tau)}{j^n \mathrm{d}\tau^n}\bigg|_{\tau=0}. \tag{5.3}$$

Let $2\sigma_i^2$ be the power in s_i. For a 2-D isotropic scattering environment, the values of $b_{i,0}$ and $b_{i,2}$ are given by [20]

$$b_{i,0} = \sigma_i^2 + \frac{N_o B_w}{2} \tag{5.4a}$$

$$b_{i,2} = 2\pi^2\sigma_i^2 f_D^2 + \frac{2\pi^2 N_o B_w^3}{3}. \tag{5.4b}$$

5.2 Rician Fading Channels

In the case where $s_i(t)$ in (5.1) is a complex Gaussian random process with non-zero mean, i.e. there exists a specular or a LOS component, $x_i(t)$ and $y_i(t)$ in (5.2) are also Gaussian random processes with non-zero means, m_{x_i} and m_{y_i}, respectively. We assume that $x_i(t)$ and $y_i(t)$ are uncorrelated and have identical variance $b_{i,0}$. Then the magnitude of the received complex signal envelope has a Rician distribution given by [1, eq. (2.45)]

$$f_{R_i}(r_i) = \frac{r_i}{b_{i,0}} \exp\left(-\frac{r_i^2 + a_i^2}{2b_{i,0}}\right) I_0\left(\frac{r_i a_i}{b_{i,0}}\right) \tag{5.5}$$

where

$$a_i^2 = m_{x_i}^2 + m_{y_i}^2$$

is the power in the LOS component. The Rice factor, K_i, is the ratio of the power in the LOS component to the power in the scattering component given by

$$K_i = \frac{a_i^2}{2\sigma_i^2}. \tag{5.6}$$

Define the SNR, γ_i, as

$$\gamma_i = \frac{a_i^2 + 2\sigma_i^2}{N_o B_w}. \tag{5.7}$$

In the case where two fading channels are independent, the expression for dual selection diversity switching rate is given by (4.3)

$$R_{SW}^{sc} = 2f_Z(0)\int_0^\infty \dot{z} f_{\dot{Z}}(\dot{z})\mathrm{d}\dot{z} \tag{5.8}$$

where

$$f_Z(0) = \int_0^\infty f_{R_1}(r) f_{R_2}(r)\mathrm{d}r. \tag{5.9}$$

Putting (5.5) into (5.9) gives

$$f_Z(0) = \int_0^\infty \frac{r^2}{\sigma_1^2\sigma_2^2}\beta_1\beta_2 \exp\left[-\frac{r^2}{2}\left(\frac{\beta_1}{\sigma_1^2}+\frac{\beta_2}{\sigma_2^2}\right) - K_1\beta_1 - K_2\beta_2\right] \times I_0\left(\frac{r}{\sigma_1}\beta_1\sqrt{2K_1}\right) I_0\left(\frac{r}{\sigma_2}\beta_2\sqrt{2K_2}\right) \mathrm{d}r. \tag{5.10}$$

When the scattering components are statistically identical, i.e. $\sigma_1 = \sigma_2 = \sigma$ and the Rice factors are the same, i.e. $K_1 = K_2 = K$, (5.10) can be solved in closed-form. One has

$$f_Z(0) = \int_0^\infty \frac{r^2}{\sigma^4}\beta^2 \exp\left[-r^2\left(\frac{\beta}{\sigma^2}\right) - 2K\beta\right] \times I_0^2\left(\frac{r}{\sigma}\beta\sqrt{2K}\right) \mathrm{d}r. \tag{5.11}$$

Using (4.8) and [4, (6.631.1)], (5.11) can be evaluated as

$$\begin{aligned} f_Z(0) &= \int_0^\infty \frac{r^2}{\sigma^4}\beta^2 \exp\left[-r^2\left(\frac{\beta}{\sigma^2}\right) - 2K\beta\right] \times J_0^2\left(\frac{jr}{\sigma}\beta\sqrt{2K}\right) \mathrm{d}r \\ &= \frac{\sqrt{\pi\beta}}{4\sigma}\exp(-2\beta K)\, {}_3F_3\left(\frac{1}{2}, 1, \frac{3}{2}; 1, 1, 1; 2K\beta\right) \end{aligned} \tag{5.12}$$

and using [4, (9.14.1)], (5.12) can be further simplified as

$$\begin{aligned} f_Z(0) &= \frac{\sqrt{\pi\beta}}{4\sigma}\exp(-2\beta K) \sum_{k=0}^{\infty} \frac{(\frac{1}{2})_k (1)_k (\frac{3}{2})_k}{(1)_k (1)_k (1)_k} \frac{(2K\beta)^k}{k!} \\ &= \frac{\sqrt{\pi\beta}}{4\sigma}\exp(-2\beta K) \sum_{k=0}^{\infty} \frac{(\frac{1}{2})_k (\frac{3}{2})_k}{(1)_k (1)_k} \frac{(2K\beta)^k}{k!} \\ &= \frac{\sqrt{\pi\beta}}{4\sigma}\exp(-2\beta K)\, {}_2F_2\left(\frac{1}{2}, \frac{3}{2}; 1, 1; 2K\beta\right). \end{aligned} \tag{5.13}$$

Since the noise n_i is independent of s_i, independence between r_i and $\dot{r}_i$ holds. Then from (2.7), $\dot{z}$ has a Gaussian distribution with zero-mean because $\dot{r}_1$ and $\dot{r}_2$ are independent zero-mean Gaussian processes [10]. The PDF of $\dot{r}_i$ is given by [1]

$$f_{\dot{R}_i}(\dot{r}_i) = \frac{1}{\sqrt{2\pi b_{i,2}}}\exp\left(-\frac{\dot{r}_i^2}{2b_{i,2}}\right). \tag{5.14}$$

Then, one obtains the PDF of $\dot{Z}$ as

$$f_{\dot{Z}}(\dot{z}) = \frac{1}{\sqrt{2\pi}\sigma_{\dot{z}}}\exp\left(-\frac{\dot{z}^2}{2\sigma_{\dot{z}}^2}\right) \tag{5.15}$$

where

$$\sigma_{\dot{z}}^2 = b_{1,2} + b_{2,2}$$
$$= 2\pi^2 f_D^2 \left\{ \sigma_1^2 \left[1 + \frac{2}{3}\left(\frac{B_w}{f_D}\right)^2 \left(\frac{1}{\beta_1} - 1\right) \right] + \sigma_2^2 \left[1 + \frac{2}{3}\left(\frac{B_w}{f_D}\right)^2 \left(\frac{1}{\beta_2} - 1\right) \right] \right\}. \tag{5.16}$$

Substituting (5.15) into the integral in (5.8) yields

$$\int_0^\infty \dot{z} f_{\dot{Z}}(\dot{z}) \mathrm{d}\dot{z} = \int_0^\infty \frac{\dot{z}}{\sqrt{2\pi}\sigma_{\dot{z}}} \exp\left(-\frac{\dot{z}^2}{2\sigma_{\dot{z}}^2}\right) \mathrm{d}\dot{z}$$
$$= \frac{\sigma_{\dot{z}}}{\sqrt{2\pi}} \tag{5.17}$$

where [4, (3.461.3)] is used. Combining (5.17) and (5.13) with (5.8) yields an exact expression for the switching rate of dual selection diversity in noisy Rician fading channels. For dual i.i.d. diversity branches, the switching rate normalized by f_D is simplified as

$$R_{SW}^{sc}/f_D = \pi \sqrt{\frac{\gamma}{2(\gamma+K+1)}} \exp\left(-\frac{2K\gamma}{\gamma+K+1}\right)$$
$$\times {}_2F_2\left(\frac{1}{2}, \frac{3}{2}; 1, 1; \frac{2K\gamma}{\gamma+K+1}\right) \sqrt{1 + \frac{2}{3\gamma}\left(\frac{B_w}{f_D}\right)^2 (K+1)}. \tag{5.18}$$

It is observed that the normalized switching rate of dual selection diversity in noisy i.i.d. Rician fading channels depends on the Rice factor, the signal-to-noise ratio, and the ratio of the bandwidth of the receiver filter to the maximum Doppler frequency. At large values of SNR, (5.18) becomes

$$\lim_{\gamma\to\infty} R_{SW}^{sc}/f_D$$
$$= \lim_{\gamma\to\infty} \pi \sqrt{\frac{1}{2+2K/\gamma+2/\gamma}} \exp\left(-\frac{2K}{1+K/\gamma+1/\gamma}\right)$$
$$\times {}_2F_2\left(\frac{1}{2}, \frac{3}{2}; 1, 1; \frac{2K}{1+K/\gamma+1/\gamma}\right) \sqrt{1 + \frac{2}{3\gamma}\left(\frac{B_w}{f_D}\right)^2 (K+1)}$$
$$= \frac{\pi}{\sqrt{2}} \exp(-2K) {}_2F_2\left(\frac{1}{2}, \frac{3}{2}; 1, 1; 2K\right). \tag{5.19}$$

This result was obtained in [10, TABLE I] for a noise-free environment.

5.3 Rayleigh Fading Channels

Setting $K_1 = K_2 = 0$ in (5.10) yields the Rayleigh case. One has

$$f_Z(0) = \int_0^\infty \frac{r^2}{\sigma_1^2\sigma_2^2}\beta_1\beta_2 \exp\left[-\frac{r^2}{2}\left(\frac{\beta_1}{\sigma_1^2}+\frac{\beta_2}{\sigma_2^2}\right)\right] dr \tag{5.20}$$

where

$$\beta_i = \frac{\gamma_i}{\gamma_i+1}$$
$$\gamma_i = \frac{2\sigma_i^2}{N_o B_w}.$$

Using [4, (3.478.1)], (5.20) can be solved as

$$f_Z(0) = \frac{\sqrt{2\pi}\beta_1\beta_2\sigma_1\sigma_2}{2(\beta_1\sigma_2^2+\beta_2\sigma_1^2)^{3/2}}. \tag{5.21}$$

Substituting (5.21) and (5.16) into (5.8) gives a closed-form solution for the normalized switching rate of dual selection diversity in noisy Rayleigh fading channels of dissimilar powers, and after some algebraic manipulations, one obtains

$$R_{SW}^{sc}/f_D = \sqrt{2}\pi c_\sigma \frac{\sqrt{\gamma_1(\gamma_1+1)(\gamma_1+1/c_\sigma^2)}}{(\gamma_1+c_\sigma^2\gamma_1+2)^{3/2}}\sqrt{1+c_\sigma^2+\frac{4}{3\gamma_1}\left(\frac{B_w}{f_D}\right)^2} \tag{5.22}$$

where

$$c_\sigma = \frac{\sigma_2}{\sigma_1}.$$

One observes that the normalized switching rate of dual selection diversity in noisy Rayleigh fading channels is affected by the ratio of the scattering component powers in the two branches, the signal-to-noise ratio, and the ratio of the bandwidth of the receiver filter to the maximum Doppler frequency. At large SNR, (5.22) becomes

$$\lim_{\gamma_1\to\infty} R_{SW}^{sc}/f_D = \frac{\sqrt{2}\pi c_\sigma}{1+c_\sigma^2}. \tag{5.23}$$

In the case of i.i.d. branches, i.e. $\sigma_1 = \sigma_2$, (5.22) specializes to

$$R_{SW}^{sc}/f_D = \pi\sqrt{\frac{\gamma}{2(\gamma+1)}\left[1+\frac{2}{3\gamma}\left(\frac{B_w}{f_D}\right)^2\right]}. \tag{5.24}$$

Since ${}_2F_2(\cdot,\cdot;\cdot,\cdot;0) = 1$, and setting $K = 0$ in (5.18) yields the same expression as (5.24). At large SNR, (5.24) becomes

$$\begin{aligned}
&\lim_{\gamma\to\infty} R_{SW}^{sc}/f_D \\
&= \lim_{\gamma\to\infty} \pi\sqrt{\frac{1}{2+2/\gamma}\left[1+\frac{2}{3\gamma}\left(\frac{B_w}{f_D}\right)^2\right]} \\
&= \frac{\pi}{\sqrt{2}}.
\end{aligned} \tag{5.25}$$

The results (5.23) and (5.25) were obtained in [10, TABLE I] for a noise-free environment.

5.4 Numerical Results

Numerical results are presented by plotting the normalized switching rate, R_{SW}^{sc}/f_D, versus the signal-to-noise ratio, γ. Figs. 5.2 - 5.5 show that the switching rate in noisy fading channels converges to that in the absence of noise for large values of SNR, as expected. The normalized switching rates increase as the ratio of the bandwidth of the receiver filter to the maximum Doppler frequency increases. This interesting and useful result indicates that an adaptive filter can be used at the receiver to avoid excessive switching.

Fig. 5.2 shows normalized switching rates of dual selection combining in i.i.d. Rayleigh fading branches in the presence of noise. The normalized switching rates can be greater or lesser than those in the absence of noise, depending on the ratio, B_w/f_D, and the SNR. Generally, the switching rate in noise is greater than without noise unless the receiver filter bandwidth is narrow compared to the maximum Doppler frequency. However, the difference is small above, say, 15 dB. Fig. 5.3 shows normalized switching rates of dual selection combining in i.n.d. Rayleigh fading branches in the presence of noise when $c_\sigma = 0.5$. Comparing the results in Fig. 5.3 with those in Fig. 5.2, one observes that unequal branch powers cause the switching rate to be smaller because the branch with the greater power

becomes preferred. Again, the noise has a relatively small effect on the switching rate when the SNR of branch one is greater than about 15 dB. Fig. 5.4 shows normalized switching rates of dual selection combining in i.i.d. Rician fading branches in the presence of noise when $K = 1$ and $K = 5$. The normalized switching rates in noise have small vacillations around the switching rates without noise when the receiver filter bandwidth is comparable to the Doppler frequency for both $K = 1$ and $K = 5$; otherwise, the switching rate is generally increased by noise. The effect of noise is relatively small when the SNR is above around 20 dB for $K = 1$, and around 25 dB for $K = 5$. Fig. 5.5 shows normalized switching rates of dual selection combining in i.n.d. Rician fading branches in the presence of noise when $K_1 = 1,\ K_2 = 5,\ c_\sigma = 1$ and $K_1 = K_2 = 5,\ c_\sigma = 1/3$. In general, the normalized switching rates at small SNR are much greater than the switching rates in a noise-free environment. For example, at 0 dB SNR, the switching rate is increased 6.55, 3.93 and 2.62 times for $B_w/f_D = 5,\ 3$ and 2, respectively, for $K_1 = 1,\ K_2 = 5,\ c_\sigma = 1$. However, the difference is small when the SNR of branch one is greater than around 15 dB for all cases in Fig. 5.5.

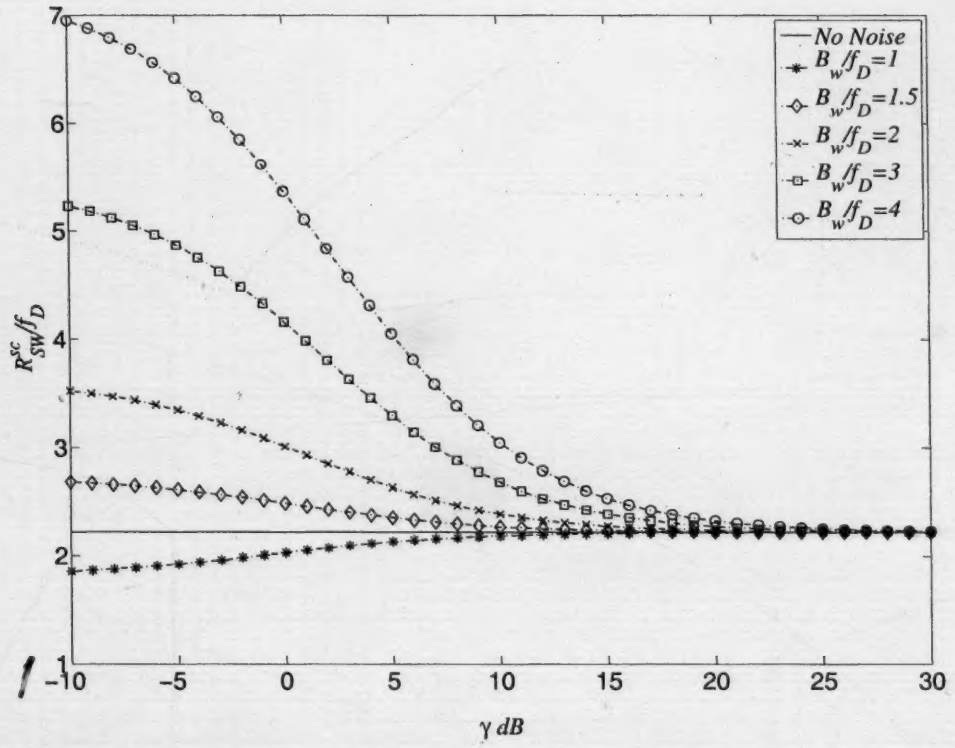

Fig. 5.2. Normalized switching rates of dual selection combining in i.i.d. Rayleigh fading branches in the presence of noise.

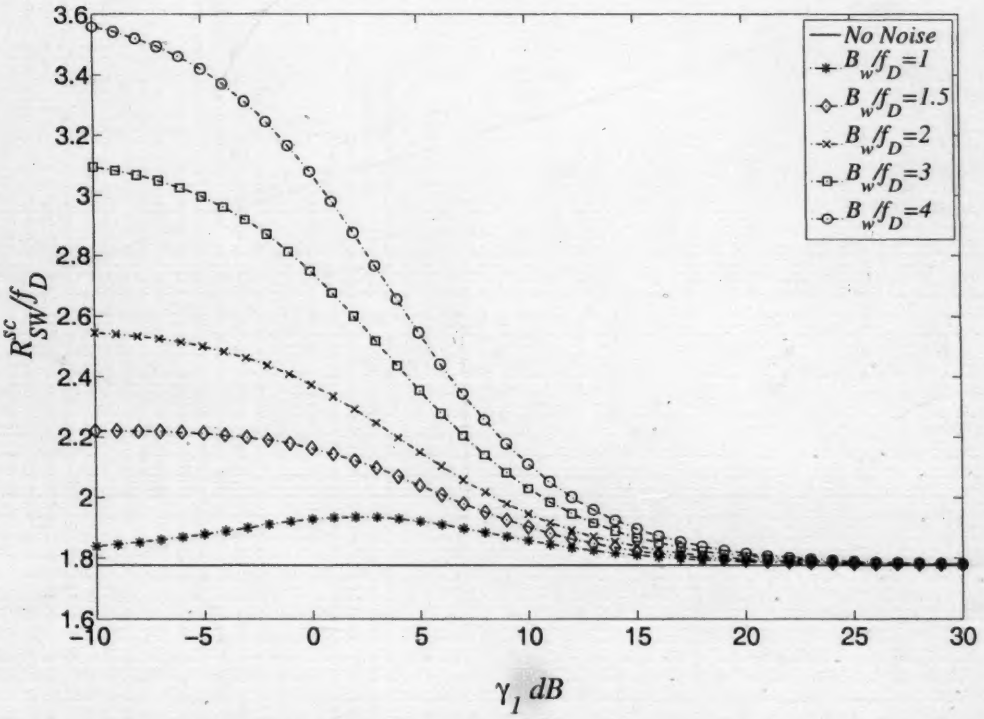

Fig. 5.3. Normalized switching rates of dual selection combining in i.n.d. Rayleigh fading branches in the presence of noise for $c_\sigma = 0.5$ ($\gamma_1 = 4\gamma_2$).

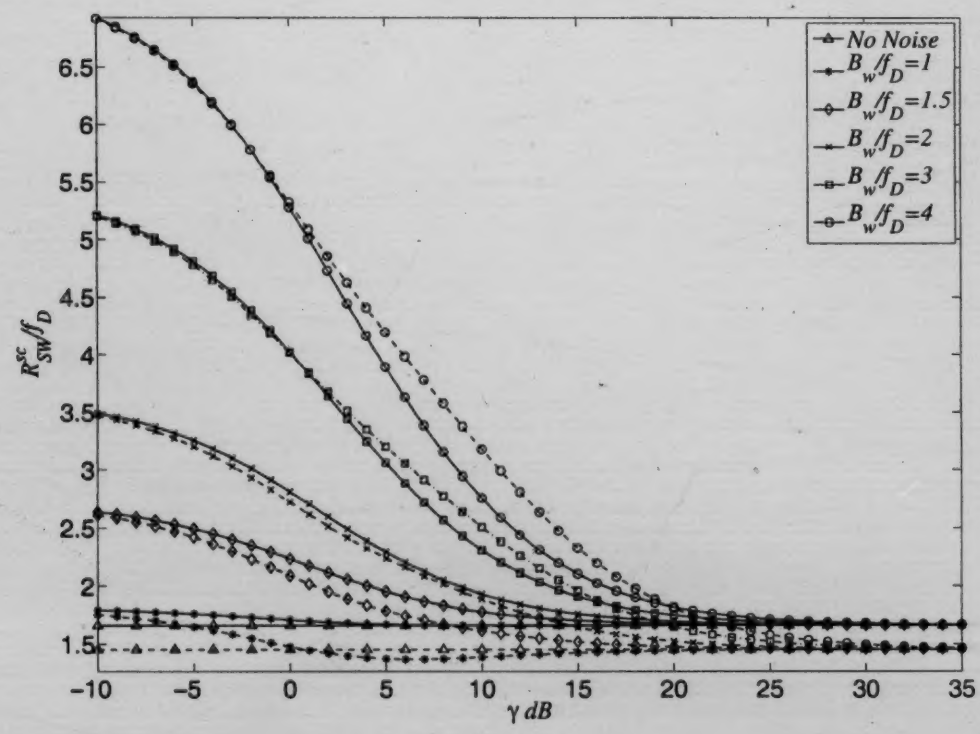

Fig. 5.4. Normalized switching rates of dual selection combining in i.i.d. Rician fading branches in the presence of noise when $K = 1$ (solid line), and $K = 5$ (dashed line).

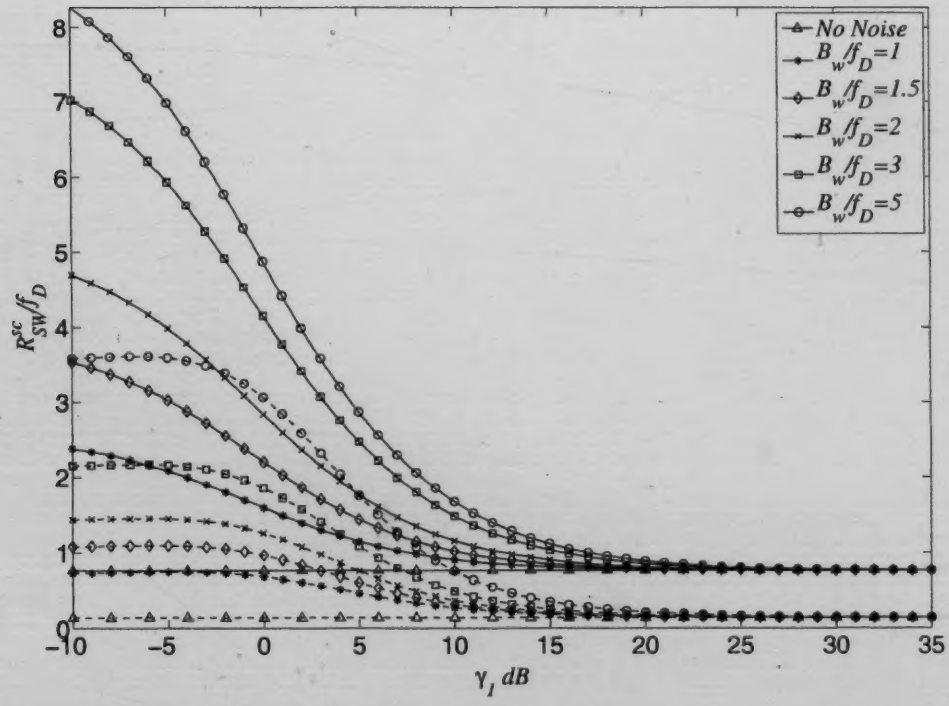

Fig. 5.5. Normalized switching rates of dual selection combining in i.n.d. Rician fading branches in the presence of noise when $K_1 = 1$, $K_2 = 5$, $c_\sigma = 1$ (solid line) and $K_1 = K_2 = 5$, $c_\sigma = 1/3$ (dashed line).

Chapter 6

Summary and Conclusions

Multipath propagation causes signal fading, which degrades the quality of service in wireless communications. Diversity combining is a powerful technique for providing better performance in signal transmission over multipath fading channels. Selection diversity combining is one widely used technique in receivers because of its simple and economical designs. A dual selection diversity combiner chooses one branch with stronger signal power from two diversity branches. The switching rate of the diversity combining helps assess receiver outages due to switching transients. If the receiver switches too often, much of the transmitted data will be lost since each switching transient corrupts the receiver filters. Also importantly, the switching rate provides valuable information for phase estimation in coherent demodulation receivers, as a coherent receiver is required to dwell on the received signal long enough in order to establish an accurate phase estimate for fading compensation. If the receiver experiences a very fast switching rate, the receiver cannot produce an accurate phase estimate. Whether branch selection is based on a symbol, multiple symbol, block or frame basis is determined by the switching rate. Power consumption is also a concern in battery-powered mobile terminals since switching branches consumes power. Motivated by the above reasons, we have examined the diversity switching rate in

this thesis.

Previous work on diversity switching rate has only considered independent Rayleigh, Rician and Nakagami-*m* fading channels in the absence of noise. In this thesis, we have extended the investigation from independent Rayleigh and Rician cases to correlated Rayleigh and Rician branches without the consideration of noise. Second, we have studied the switching rate of the selection diversity combining in i.i.d. κ-μ and α-μ distributed fading. Third, we have taken noise into account in the derivation of the switching rate in independent Rayleigh and Rician fading channels.

In summary,

1. In practical wireless communications, the fading signals received at the different antennas may be correlated due to close antenna spacing. We have considered restricted space applications in Chapter 3, where the two fading branches are correlated. An analytical expression for the selection diversity switching rate has been derived for dual correlated fading channels in the absence of noise. Both balanced and unbalanced fading channels were considered. Numerical results were presented for a space-diversity system with horizontally spaced omnidirectional antennas at a mobile terminal. It was observed that the switching rate for correlated dual diversity branches can be either greater or lesser than that for the case of independent diversity branches, depending on the angle between the antenna axis and the direction of vehicle motion and the antenna spacing.

2. The κ-μ and α-μ fading models provide better fits to field measurements than other traditional fading models, such as Rayleigh, Rician and Nakagami-*m*. They also fully describe the characteristics of the fading signal in terms of measurable physical parameters. A closed-form expression for the switching rate has been derived for dual selection diversity combining, which is a new unifying result that is more general

than previous results and includes them as special cases. Dual i.i.d. κ-μ and α-μ fading channels have been adopted, and numerical results have been presented.

3. In practical communication systems, noise is unavoidable and it degrades the quality of transmitted signals. Therefore, it is important to explore the effects of noise on the switching rate in fading channels. An analytical expression for the switching rate has been derived for dual selection diversity combining in the presence of noise. Both i.i.d. and i.n.d. fading channels have been considered, and numerical results have been presented. It was observed that the switching rate in noisy fading channels converges to that in the absence of noise at high SNR, and an adaptive filter can be used at the receiver to adjust the bandwidth of the receiver filter to avoid excessive switching.

Appendix A

Equivalence of the κ-μ Distribution and the Generalized Rician Distribution

In this appendix, we will show that (1.20) is a version of the generalized Rician distribution. Let R be defined as

$$R = \sqrt{\sum_{j=1}^{n'} X_j^2} \tag{A-1}$$

where X_j are independent Gaussian random variables with means m_j, $j = 1,2,\cdots,n'$ and identical variances σ^2. Then the generalized Rician distribution has the PDF given in [22, eq. (2.1-143)]

$$f_R(r) = \frac{r^{n'/2}}{\sigma^2 a^{(n'-2)/2}} \exp\left[-\frac{r^2+a^2}{2\sigma^2}\right] I_{n'/2-1}\left(\frac{ra}{\sigma^2}\right) \tag{A-2}$$

where

$$a^2 = \sum_{j=1}^{n'} m_j^2,$$

which is equivalent to d^2, and $r \geq 0$. The second moment of R is given in [22, eq. (2.1-146)]

$$E(R^2) = 2\sigma^2 \exp\left(-\frac{a^2}{2\sigma^2}\right) \frac{\Gamma(n'/2+1)}{\Gamma(n'/2)} {}_1F_1\left(\frac{n'}{2}+1, \frac{n'}{2}; \frac{a^2}{2\sigma^2}\right). \tag{A-3}$$

Note that (1.18) is the summation of $2n$ independent non-zero mean Gaussian random variables. Therefore, replacing n' in (A-1) with $2n$, one can write (A-2) as

$$f_R(r) = \frac{r^n}{\sigma^2 a^{n-1}} \exp\left[-\frac{r^2+a^2}{2\sigma^2}\right] I_{n-1}\left(\frac{ra}{\sigma^2}\right) \tag{A-4}$$

and (A-3) as

$$E(R^2) = 2\sigma^2 \exp\left(-\frac{a^2}{2\sigma^2}\right) \frac{\Gamma(n+1)}{\Gamma(n)} {}_1F_1\left(n+1, n; \frac{a^2}{2\sigma^2}\right). \tag{A-5}$$

Next, we will show that (A-5) is identical to $\hat{r}^2$ in (1.20). Using [4, (9.14.1)] and [4, (8.331.1)], (A-5) can be written as

$$E(R^2) = 2\sigma^2 \exp\left(-\frac{a^2}{2\sigma^2}\right) \sum_{k=0}^{\infty} (n+k) \frac{\left(\frac{a^2}{2\sigma^2}\right)^k}{k!}. \tag{A-6}$$

Combining the identity

$$e^x = \sum_{n=0}^{\infty} \frac{x^n}{n!}$$

with (A-6) and after some simplifications, one obtains

$$E(R^2) = 2\sigma^2 n + a^2. \tag{A-7}$$

In (1.20), μ is the real extension of integer n. Substituting $\mu = n$, $\hat{r} = \sqrt{2n\sigma^2 + d^2}$ and $d^2 = a^2$ into (1.20) yields (A-4) after some algebraic manipulations.

Appendix B

Derivation of Conditional Mean and Variance of $\dot{\mathbf{S}}$ in Rayleigh Fading

In this appendix, we will derive $\mathbf{M} = \mathbb{E}[\dot{\mathbf{S}}|\mathbf{S}]$ and $\Lambda = \mathrm{Var}[\dot{\mathbf{S}}|\mathbf{S}]$ for dual selection diversity combining in Rayleigh fading channels. Define the matrices $\dot{\mathbf{S}} = [\dot{S}_1,\ \dot{S}_2]^T$ and $\mathbf{S} = [S_1,\ S_2]^T$, where $(\cdot)^T$ denotes the transpose matrix. Here $\dot{S}_1$, $\dot{S}_2$, S_1 and S_2 are mutually correlated Complex Gaussian variables. Then the matrices $\mathbf{M}$ and Λ are given by [15, eq. (22)]

$$\begin{aligned} \mathbf{M} &= \mu\mathbf{S} = (\mathbf{c}\mathbf{b}^{-1})^*\mathbf{S} \\ \Lambda &= \mathbf{a} - \mathbf{c}\mathbf{b}^{-1}\mathbf{c}^{T*} \end{aligned} \tag{B-1}$$

where $(\cdot)^{-1}$ denotes the inverse matrix, $\mathbf{a}$, $\mathbf{b}$ and $\mathbf{c}$ are partitioned matrices of the matrix

$$\frac{1}{2}\begin{bmatrix}\dot{\mathbf{S}}\\ \mathbf{S}\end{bmatrix}^*\begin{bmatrix}\dot{\mathbf{S}}\\ \mathbf{S}\end{bmatrix}^T = \begin{bmatrix}\mathbf{a} & \mathbf{c}\\ \mathbf{a}^{*T} & \mathbf{b}\end{bmatrix}. \tag{B-2}$$

Let $\rho_{ij}(\tau) = \mathbb{E}[S_i^*(t)S_j(t+\tau)]$, then $\dot{\rho}_{ij}(\tau)$ is the first derivative of $\rho_{ij}(\tau)$ with respect to τ, $\ddot{\rho}_{ij}(\tau)$ is the second derivative of $\rho_{ij}(\tau)$ with respect to τ, $\rho_{ij} = \rho_{ij}(0)$, $\dot{\rho}_{ij} = \dot{\rho}_{ij}(0)$,

and $\ddot{\rho}_{ij} = \ddot{\rho}_{ij}(0)$. Then μ and Λ can be obtained as

$$\mu = \frac{1}{1-|\rho_{12}|^2}\begin{bmatrix} \dot{\rho}_{12}^*\rho_{12} & -\dot{\rho}_{12}^* \\ \dot{\rho}_{12} & -\dot{\rho}_{12}\rho_{12}^* \end{bmatrix}$$

$$\Lambda = -\frac{1}{2}\begin{bmatrix} \ddot{\rho}_{11} + \frac{|\dot{\rho}_{12}|^2}{1-|\rho_{12}|^2} & \ddot{\rho}_{12} + \frac{\rho_{12}^*(\dot{\rho}_{12})^2}{1-|\rho_{12}|^2} \\ \ddot{\rho}_{12}^* + \frac{\rho_{12}(\dot{\rho}_{12}^*)^2}{1-|\rho_{12}|^2} & \ddot{\rho}_{11} + \frac{|\dot{\rho}_{12}|^2}{1-|\rho_{12}|^2} \end{bmatrix}. \tag{B-3}$$

Then it follows that

$$\mathbf{M} = \frac{1}{1-|\rho_{12}|^2}\begin{bmatrix} \dot{\rho}_{12}^*\rho_{12}S_1 - \dot{\rho}_{12}^*S_2 \\ \dot{\rho}_{12}S_1 - \dot{\rho}_{12}\rho_{12}^*S_2 \end{bmatrix}. \tag{B-4}$$

Appendix C

Derivation of Conditional Mean and Variance of $\dot{\mathbf{R}}$ in Rician Fading

In this appendix, we will derive $\mathbf{M} = \mathbb{E}[\dot{\mathbf{R}}|\mathbf{R}]$ and $\Lambda = \mathbb{E}[\dot{\mathbf{R}}\dot{\mathbf{R}}^T|\mathbf{R}] - \mathbb{E}[\dot{\mathbf{R}}|\mathbf{R}]\mathbb{E}[\dot{\mathbf{R}}^T|\mathbf{R}]$ for dual selection diversity combining in Rician fading channels. Define the matrices $\dot{\mathbf{R}} = [\dot{X}_1,\ \dot{Y}_1,\ \dot{X}_2,\ \dot{Y}_2]^T$ and $\mathbf{R} = [X_1,\ Y_1,\ X_2,\ Y_2]^T$. Here $\dot{X}_1$, $\dot{Y}_1$, $\dot{X}_2$, $\dot{Y}_2$, X_1, Y_1, X_2 and Y_2 are jointly correlated Gaussian variables. Then the matrices $\mathbf{M}$ and Λ are given by [17, eq. (15)]

$$\begin{aligned} \mathbf{M} &= (\mathbf{c}\mathbf{b}^{-1})(\mathbf{R}-\mathbf{m}) \\ \Lambda &= \mathbf{a} - \mathbf{c}\mathbf{b}^{-1}\mathbf{c}^T \end{aligned} \tag{C-1}$$

where $\mathbf{a}$, $\mathbf{b}$ and $\mathbf{c}$ are partitioned matrices of the matrix

$$\begin{bmatrix} \mathbf{a} & \mathbf{c} \\ \mathbf{c}^T & \mathbf{b} \end{bmatrix} = \mathbb{E}\left\{ \begin{bmatrix} \dot{\mathbf{R}} \\ \mathbf{R} \end{bmatrix} \begin{bmatrix} \dot{\mathbf{R}} \\ \mathbf{R} \end{bmatrix}^T \right\} - \mathbb{E}\left\{ \begin{bmatrix} \dot{\mathbf{R}} \\ \mathbf{R} \end{bmatrix} \right\} \mathbb{E}\left\{ \begin{bmatrix} \dot{\mathbf{R}} \\ \mathbf{R} \end{bmatrix}^T \right\}. \tag{C-2}$$

Matrices **a**, **b** and **c** can be calculated as [17, (17a)-(17d)]

$$\mathbf{a} = \begin{bmatrix} -\sigma_1^2\ddot{\mu}_a & 0 & -\sigma_1\sigma_2\ddot{\mu}_c & -\sigma_1\sigma_2\ddot{\nu}_c \\ 0 & -\sigma_1^2\ddot{\mu}_a & \sigma_1\sigma_2\ddot{\nu}_c & -\sigma_1\sigma_2\ddot{\mu}_c \\ -\sigma_1\sigma_2\ddot{\mu}_c & \sigma_1\sigma_2\ddot{\nu}_c & -\sigma_2^2\ddot{\mu}_a & 0 \\ -\sigma_1\sigma_2\ddot{\nu}_c & -\sigma_1\sigma_2\ddot{\mu}_c & 0 & -\sigma_2^2\ddot{\mu}_a \end{bmatrix} \tag{C-3a}$$

$$\mathbf{b} = \begin{bmatrix} \sigma_1^2\mu_a & 0 & \sigma_1\sigma_2\mu_c & \sigma_1\sigma_2\nu_c \\ 0 & \sigma_1^2\mu_a & -\sigma_1\sigma_2\nu_c & \sigma_1\sigma_2\mu_c \\ \sigma_1\sigma_2\mu_c & -\sigma_1\sigma_2\nu_c & \sigma_2^2\mu_a & 0 \\ \sigma_1\sigma_2\nu_c & \sigma_1\sigma_2\mu_c & 0 & \sigma_2^2\mu_a \end{bmatrix} \tag{C-3b}$$

$$\mathbf{c} = \begin{bmatrix} 0 & \sigma_1^2\dot{\nu}_a & \sigma_1\sigma_2\dot{\mu}_c & -\sigma_1\sigma_2\dot{\nu}_c \\ -\sigma_1^2\dot{\nu}_a & 0 & -\sigma_1\sigma_2\dot{\nu}_c & \sigma_1\sigma_2\dot{\mu}_c \\ -\sigma_1\sigma_2\dot{\mu}_c & \sigma_1\sigma_2\dot{\nu}_c & 0 & \sigma_2^2\ddot{\nu}_a \\ -\sigma_1\sigma_2\dot{\nu}_c & -\sigma_1\sigma_2\dot{\mu}_c & -\sigma_2^2\dot{\nu}_a & 0 \end{bmatrix} \tag{C-3c}$$

$$\mathbf{m} = [m_{X_1}\ m_{Y_1}\ m_{X_2}\ m_{Y_2}]^T \tag{C-3d}$$

where

$$\mu_a(\tau) = \frac{\mathrm{Cov}\{X_i(t+\tau), X_i(t)\}}{\sigma_i^2} = \frac{\mathrm{Cov}\{Y_i(t+\tau), Y_i(t)\}}{\sigma_i^2} \tag{C-4a}$$

$$\nu_a(\tau) = \frac{\mathrm{Cov}\{X_i(t+\tau), Y_i(t)\}}{\sigma_i^2} \tag{C-4b}$$

$$\mu_c(\tau) = \frac{\mathrm{Cov}\{X_1(t+\tau), X_2(t)\}}{\sigma_1\sigma_2} = \frac{\mathrm{Cov}\{Y_1(t+\tau), Y_2(t)\}}{\sigma_1\sigma_2} \tag{C-4c}$$

$$\nu_c(\tau) = \frac{\mathrm{Cov}\{X_1(t+\tau), Y_2(t)\}}{\sigma_1\sigma_2} = -\frac{\mathrm{Cov}\{Y_1(t+\tau), X_2(t)\}}{\sigma_1\sigma_2} \tag{C-4d}$$

and $\dot{\gamma}$, $\ddot{\gamma}$ are the first and the second derivatives of γ with respect to τ, where $\gamma = \{\mu_a, \mu_c, \nu_a, \nu_c\}$. Then (C-1) can be obtained after some algebraic manipulations [17, (19a)-(19j)]

$$\mathbf{M} = \begin{bmatrix} M_1 & -M_2 & -\frac{\sigma_1}{\sigma_2}M_3 & -\frac{\sigma_1}{\sigma_2}M_4 \\ M_2 & M_1 & \frac{\sigma_1}{\sigma_2}M_4 & -\frac{\sigma_1}{\sigma_2}M_3 \\ \frac{\sigma_2}{\sigma_1}M_3 & -\frac{\sigma_2}{\sigma_1}M_4 & -M_1 & -M_2 \\ \frac{\sigma_2}{\sigma_1}M_4 & \frac{\sigma_2}{\sigma_1}M_3 & M_2 & -M_1 \end{bmatrix} \begin{bmatrix} X_1 - m_{X_1} \\ Y_1 - m_{Y_1} \\ X_2 - m_{X_2} \\ Y_2 - m_{Y_2} \end{bmatrix} \tag{C-5a}$$

$$\Lambda = \begin{bmatrix} \sigma_1^2\Lambda_1 & 0 & \sigma_1\sigma_2\Lambda_2 & \sigma_1\sigma_2\Lambda_3 \\ 0 & \sigma_1^2\Lambda_1 & -\sigma_1\sigma_2\Lambda_3 & \sigma_1\sigma_2\Lambda_2 \\ \sigma_1\sigma_2\Lambda_2 & -\sigma_1\sigma_2\Lambda_3 & \sigma_2^2\Lambda_1 & 0 \\ \sigma_1\sigma_2\Lambda_3 & \sigma_1\sigma_2\Lambda_2 & 0 & \sigma_2^2\Lambda_1 \end{bmatrix} \tag{C-5b}$$

$$\eta^{-1} = \mu_c^2 + \nu_c^2 - \mu_a^2 \tag{C-5c}$$

$$M_1 = \eta\,(\mu_c\dot{\mu}_c + \nu_c\dot{\nu}_c) \tag{C-5d}$$

$$M_2 = \eta\,(\nu_c\dot{\mu}_c + \mu_c\dot{\nu}_a - \mu_c\dot{\nu}_c) \tag{C-5e}$$

$$M_3 = \eta\,(\mu_a\dot{\mu}_c + \nu_c\dot{\nu}_a) \tag{C-5f}$$

$$M_4 = \eta\,(\mu_a\dot{\mu}_c - \mu_c\dot{\nu}_a) \tag{C-5g}$$

$$\Lambda_1 = \eta\left[2\dot{\nu}_a(\nu_c\dot{\mu}_c - \mu_c\dot{\nu}_c) + \mu_a\left(\dot{\mu}_c^2 + \dot{\nu}_a^2 + \dot{\nu}_c^2\right)\right] - \ddot{\mu}_a \tag{C-5h}$$

$$\Lambda_2 = \eta\left[2\dot{\nu}_c(\nu_c\dot{\mu}_c - \mu_a\dot{\nu}_a) + \mu_c\left(\dot{\mu}_c^2 - \dot{\nu}_a^2 - \dot{\nu}_c^2\right)\right] - \ddot{\mu}_c \tag{C-5i}$$

$$\Lambda_3 = \eta\left[2\dot{\mu}_c(\mu_c\dot{\nu}_c - \mu_a\dot{\nu}_a) + \nu_c\left(\dot{\nu}_c^2 - \dot{\nu}_a^2 - \dot{\mu}_c^2\right)\right] - \ddot{\nu}_c. \tag{C-5j}$$

References

[1] G. L. Stüber, *Principles of Mobile Communications*, 2nd ed. Kluwer Academic Publishers, 2002.

[2] D. J. Young and N. C. Beaulieu, "The generation of correlated rayleigh random variates by inverse discrete fourier transform," *IEEE Trans. Commun.*, vol. 48, pp. 1114–1127, 2000.

[3] D. J. Young and N. C. Beaulieu, "Power margin quality measures for correlated random variates from the normal distribution," *IEEE Trans. Inform. Theory*, vol. 49, no. 1, pp. 241–252, Jan. 2003.

[4] I. S. Gradshteyn and I. M. Ryzhik, *Table of Integrals, Series, and Products*, 6th ed. San Diego: Academic Press, 2000.

[5] M. D. Yacoub, "The κ-μ distribution and the η-μ distribution," *IEEE Antennas Propag. Mag.*, vol. 49, pp. 68–81, Feb. 2007.

[6] S. L. Cotton and W. G. Scanlon, "High-order statistics for κ-μ distribution," *Electron. Lett.*, vol. 43, no. 22, Oct. 2007.

[7] M. D. Yacoub, "The α-μ distribution: a physical fading model for the stacy distribution," *IEEE Trans. Veh. Technol.*, vol. 56, no. 1, pp. 27–34, Jan. 2007.

[8] D. B. da Costa, J. C. S. S. Filho, M. D. Yacoub, and G. Fraidenraich, "Crossing rates and fade durations for diversity-combining schemes over α-μ fading chanels," *IEEE Trans. Wireless Commun.*, vol. 6, no. 12, pp. 4263–4267, Dec. 2007.

[9] S. O. Rice, "Statistical properties of a sine wave plus noise," *Bell Syst. Tech. J.*, vol. 27, pp. 109–157, 1948.

[10] N. C. Beaulieu, "Switching rates of dual selection diversity and dual switch-and-stay diversity," *to appear in IEEE Trans. Commun.*, Apr. 2008.

[11] J. K. Cavers and P. Ho, "Switching rate and dwell time in m-of-n selection diversity," *IEEE Trans. Wireless Commun.*, vol. 6, pp. 1218–1223, Apr. 2007.

[12] H.-C. Yang and M.-S. Alouini, "Markov chains and performance comparison of switched diversity systems," *IEEE Trans. Wireless Commun.*, vol. 52, pp. 1113–1125, July 2004.

[13] J. K. Cavers and P. Ho, "Switching rate and dwell time of hybrid selection-maximal ratio combining in rayleigh fading channels," in *Proc. Vehicular Technology Conference VTC 2006-Spring*, Mar. 7–10 2006, vol. 4, pp. 1650–1654.

[14] N. C. Beaulieu, "Switching rates of selection diversity and switch-and-stay diversity," in *Proc. IEEE International Conference on Communications, ICC 2008*, Beijing, China.

[15] F. Adachi, M. T. Feeney, and J. D. Parsons, "Effects of correlated fading on level crossing rates and average fade durations with predetection diversity reception," *Proc. IEE*, vol. 135, pp. 11–17, Feb. 1988.

[16] J. C. S. S. Filho, G. Fraidenraich, and M. D. Yacoub, "Exact crossing rates of dual diversity over unbalanced correlated rayleigh channels," *IEEE Commun. Lett.*, vol. 10, pp. 37–39, Jan. 2006.

[17] J. C. S. S. Filho, M. D. Yacoub, J. R. Mendes, and G. Fraidenraich, "General exact crossing rates and average fade durations of dual diversity combiners over non-identical correlated rician channels," *Proc. IEEE International Conference on Communications*, vol. 12, pp. 5634–5638, June 2006.

[18] A. Papoulis and S. U. Pillai, *Probability, Random Variables and Stochastic Processes*, 4th ed. New York: McGraw-Hill, 2002.

[19] B. P. Lathi, *Modern Digital and Analog Communication Systems*, 3rd ed. New York: Oxford University Press, 1998.

[20] H. Zhang and A. Abdi, "On the average crossing rates in selection diversity," *IEEE Trans. Wireless Commun.*, vol. 6, pp. 448–451, Feb. 2007.

[21] G. Park, D. Hong, and C. Kang, "Level crossing rate estimation with doppler adaptive noise suppression technique in frequency domain," in *Proc. Vehicular Technology Conference VTC 2003-Fall*, Oct. 6–9 2003, vol. 2, pp. 1192–1195.

[22] J. G. Proakis, *Digital Communications*, 4th ed. New York: McGraw-Hill, 2000.

Vita

Name:

Xin Wang

Education:

University of Alberta, September 2006 – present.

M.Sc. in Electrical and Computer Engineering.

University of Alberta, September 2002 – April 2006.

B.Sc. in Electrical Engineering (Graduation with Distinction).

Experience:

Research Assistant, University of Alberta, September 2006 – present,

Department of Electrical and Computer Engineering.

Teaching Assistant, University of Alberta, January – April 2008,

Department of Electrical and Computer Engineering.

Awards/Scholarships:

Alberta Learning Graduate Scholarship, 2007.

Dean's Research Award (Faculty of Engineering), 2006.

GE Fanuc Software Undergraduate Scholarship, 2005.

Dean's Research Award (Faculty of Engineering), 2005.

Canadian Gas Processors Association Silver Anniversary Scholarship, 2004.

Randy Duane Rawson Memorial Scholarship in Electrical Engineering, 2004.

IEEE Northern Canada Section Scholarship, 2004.

University of Alberta Undergraduate Scholarship, 2003.

Publications:

X. Wang and N. C. Beaulieu, "Switching Rates of Two-branch Selection Diversity in Correlated Doppler Fading," to appear in *IEEE Trans. Wireless Commun.*.

X. Wang and N. C. Beaulieu, "Switching Rates of Two-branch Selection Diversity in κ-μ and α-μ Distributed Fadings," to appear in *IEEE Trans. Wireless Commun.*.

X. Wang and N. C. Beaulieu, "Switching Rates of Dual Selection Diversity in Noisy Fading Channels," to appear in *IEEE Trans. Commun.*.